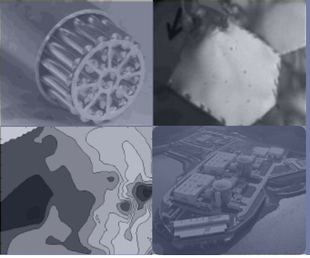

Line Profile Analysis
Characterizing crystallographic defect structures using diffraction

Levente Balogh

Department of Mechanical and Materials Engineering, Queen's University, Kingston, ON, Canada

The mechanical properties of materials determine their possible engineering applications

Berlin Central Station - Wikimedia Commons
http://wikiarquitectura.com/es/images/f/f2/Estac_tren_berlin_21.jpg

by Torsten Bätge, Wikimedia Commons - http://commons.wikimedia.org/wiki/File:Kupferfittings_4062.jpg

Structural steel
Yield strength: ~ 250-700 MPa

Copper
Yield strength: ~ 50-70 MPa

Microstructure and mechanical properties are strongly correlated

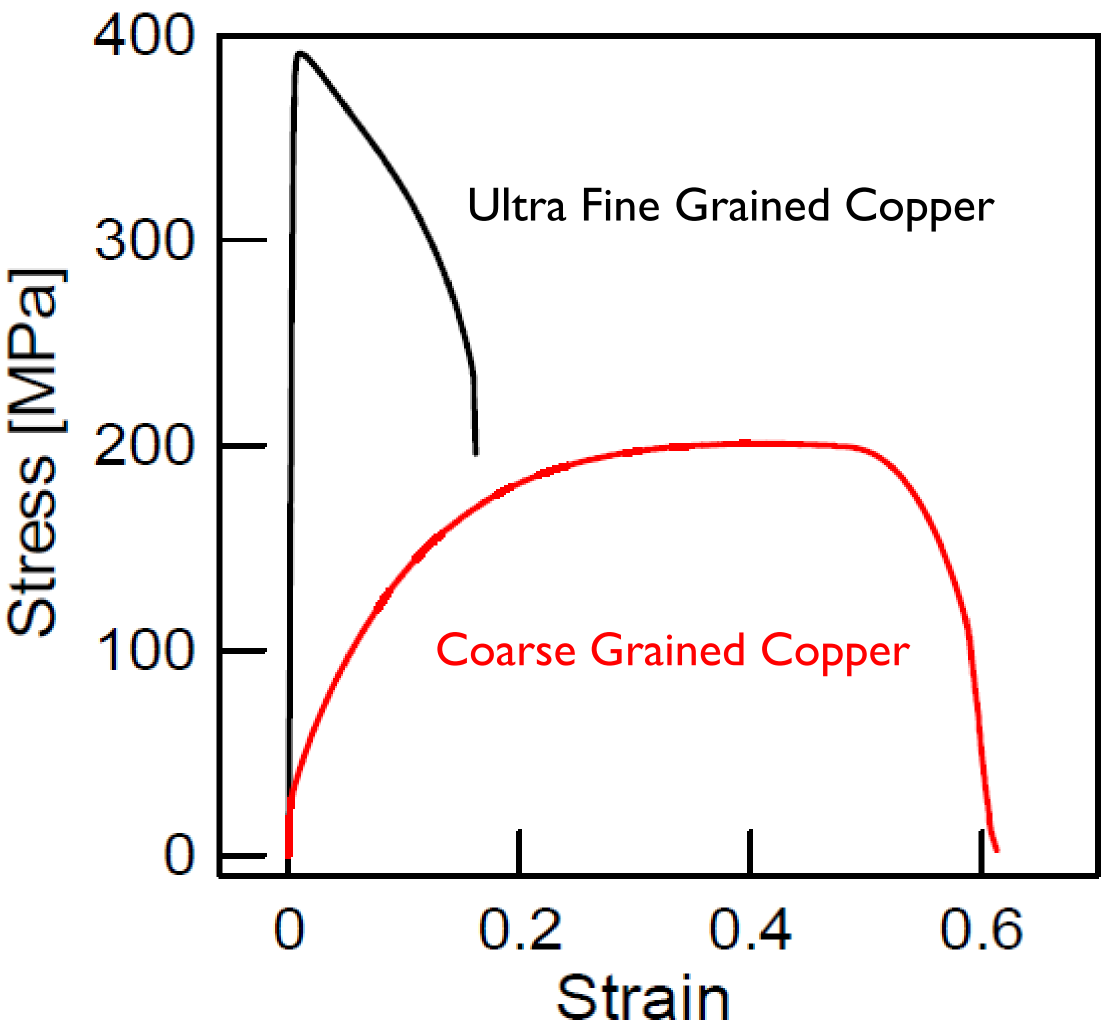

L. Kunz, L. Collini, *Frattura ed Integrita Strutturale,* 19 (2012) 61-75

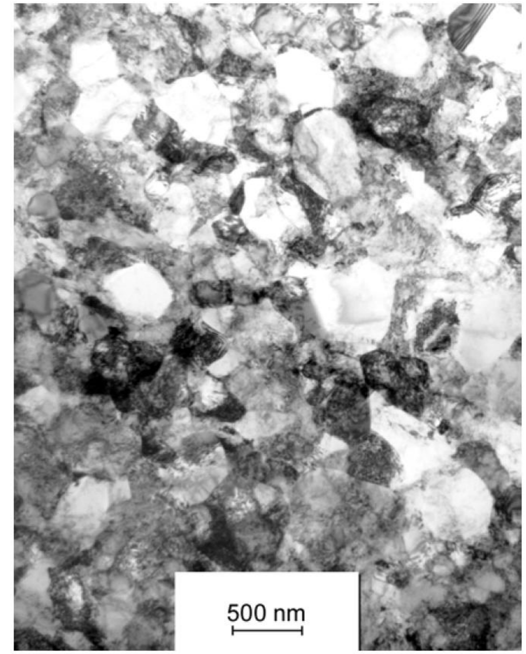

B. Hadzima, M. Janecek, R. J. Hellmig, Y. Kutnyakova & Yuri Estrin, *Mater. Sci. For.*503-504 (2006) pp 883-888.

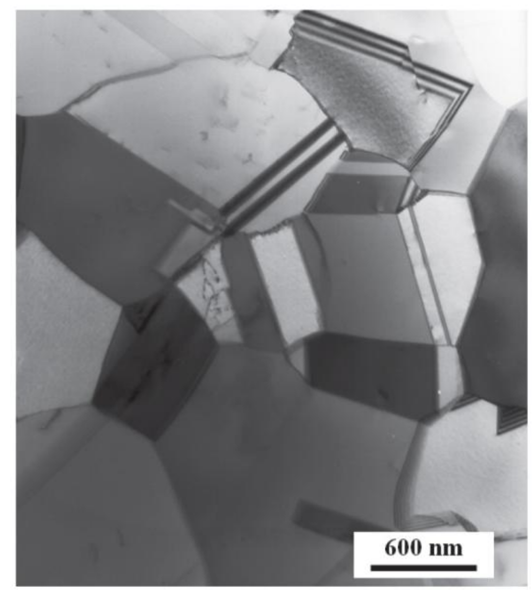

L. Mingwei, Z. Gang, Z. Yesheng, H. Fei, H. Xiaodong, *Materials Research.* 2013; 16(1): 88-93.

The mechanical properties of materials can be tailored within a wide range by varying the microstructure

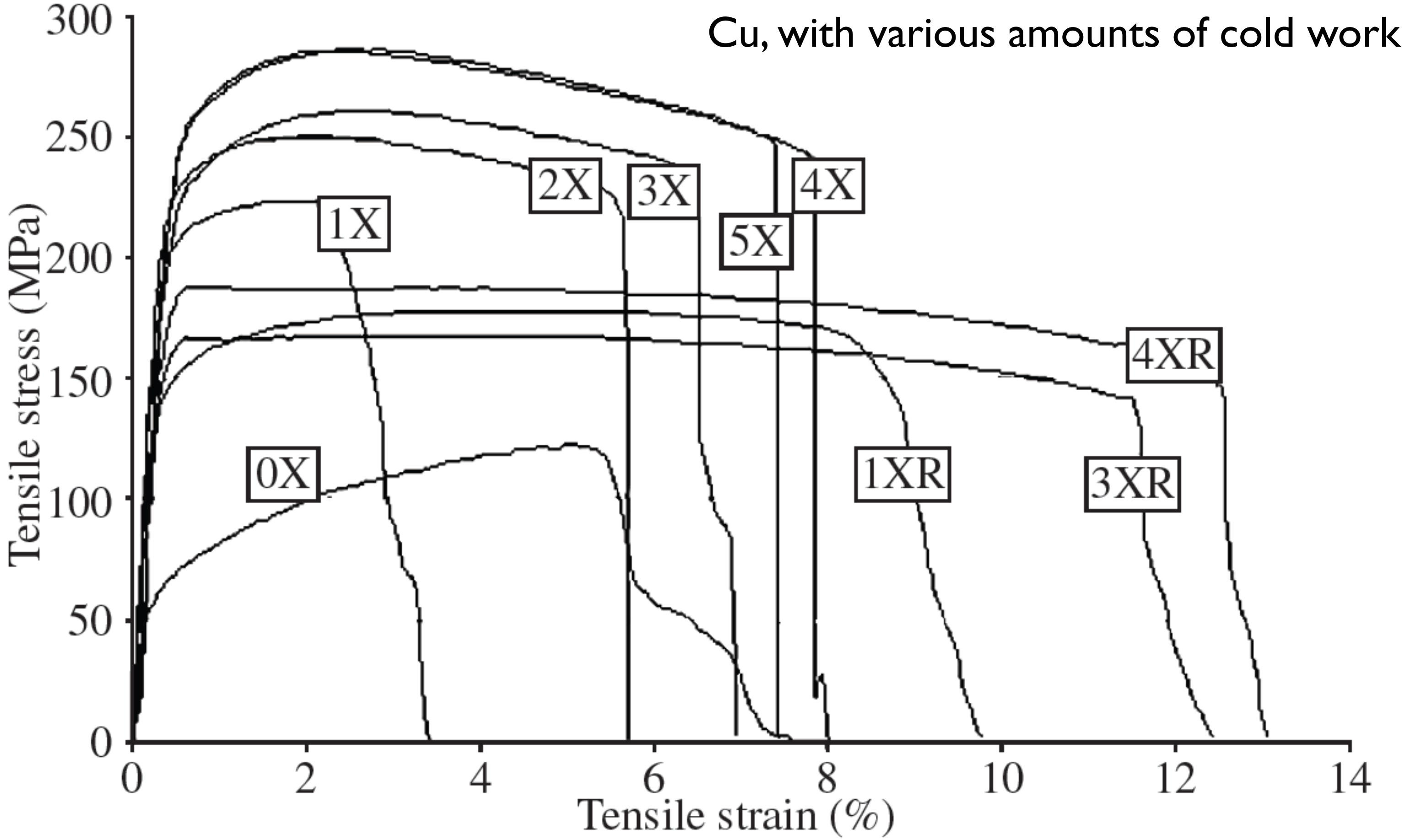

E. F. Prados, V. L. Sordi, M. Ferrante, *Materials Research*, Vol. 11, No. 2, 199-205, 2008

Diffraction peak widths and shapes are correlated to the microstructure

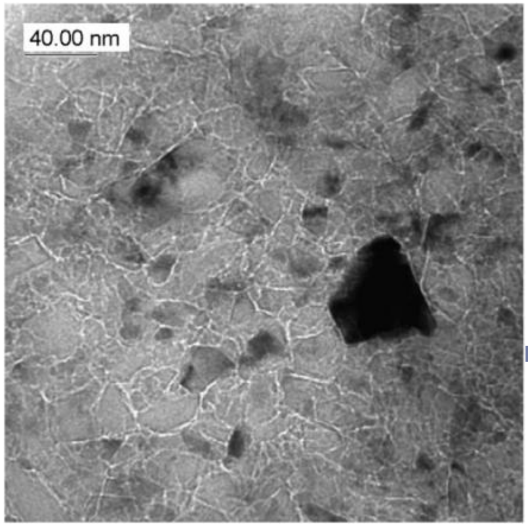

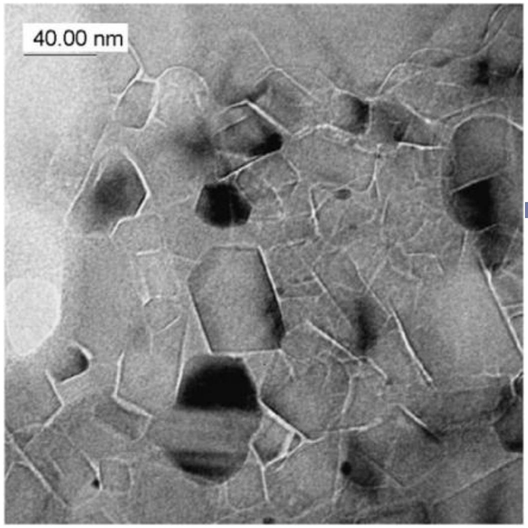

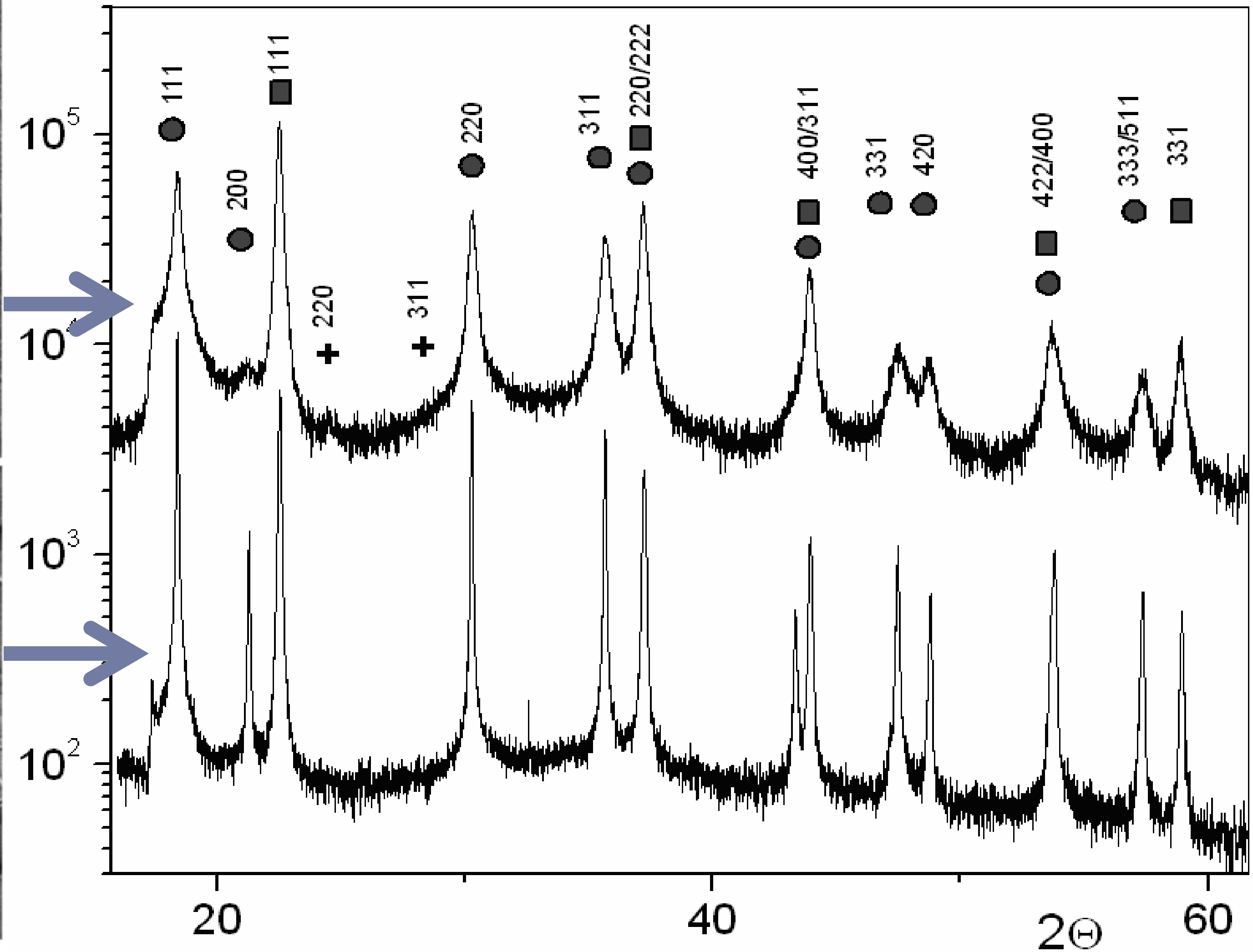

L. Balogh, S. Nauyoks, T. W. Zerda, C. Pantea, S. Stelmakh, B. Palosz, T. Ungár, *Mater. Sci. Eng. A*, 487, (2008) 180-188.

Fundamental equation of line broadening

Warren & Averbach (1952):

$$A(L) = A_{size}(L) A_{pf}(L) \exp\left(-2\pi^2 g^2 L^2 \langle \varepsilon_{L,g}^2 \rangle\right)$$

Fourier transform of a broadened diffraction peak shape

Contribution of crystallite size distribution

Contribution of planar faults

Contribution of the microstrain distribution found in the specimen

The interpretation of domain size obtained from diffraction line broadening

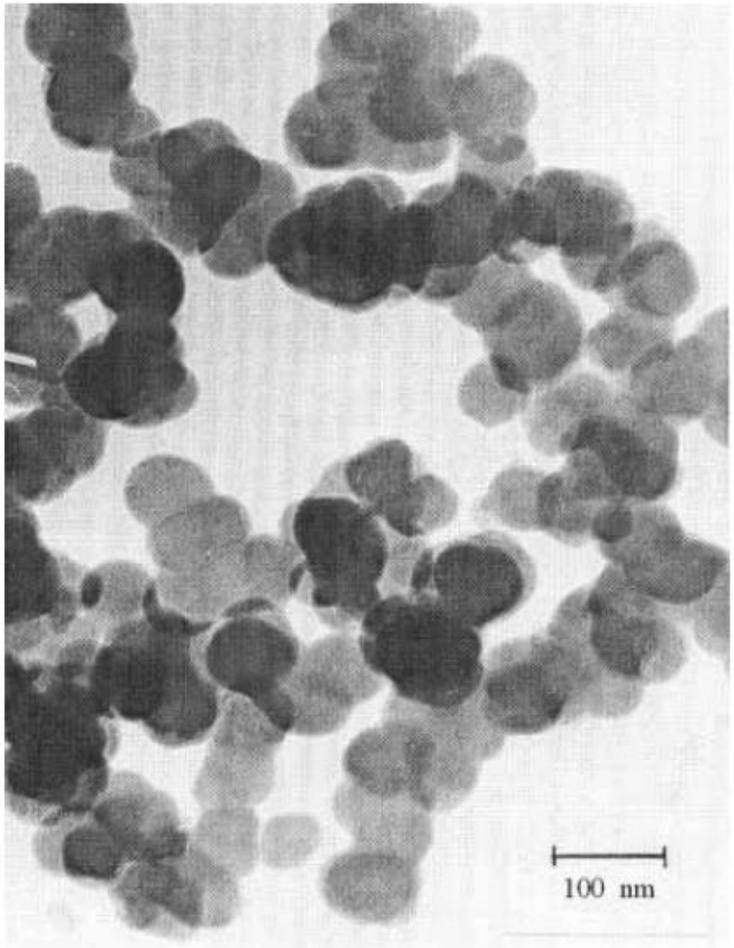

Silicon nitride powder

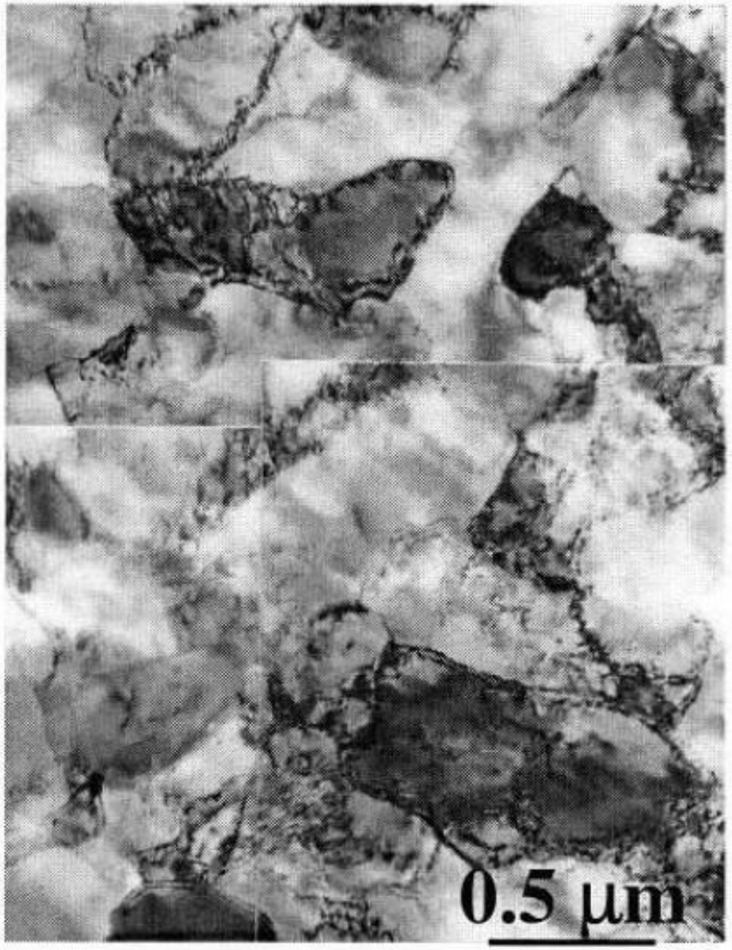

Plastically deformed Cu sample

T. Ungár, J. Gubicza, G. Ribárik and A. Borbély, *J. Appl. Cryst.* (2001) **34**, 298-310.

Powder or bulk polycrystalline materials produced without severe deformation

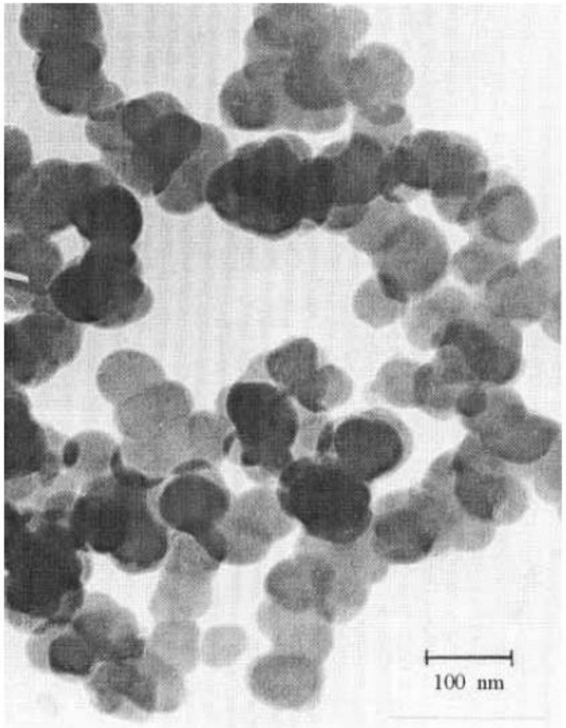

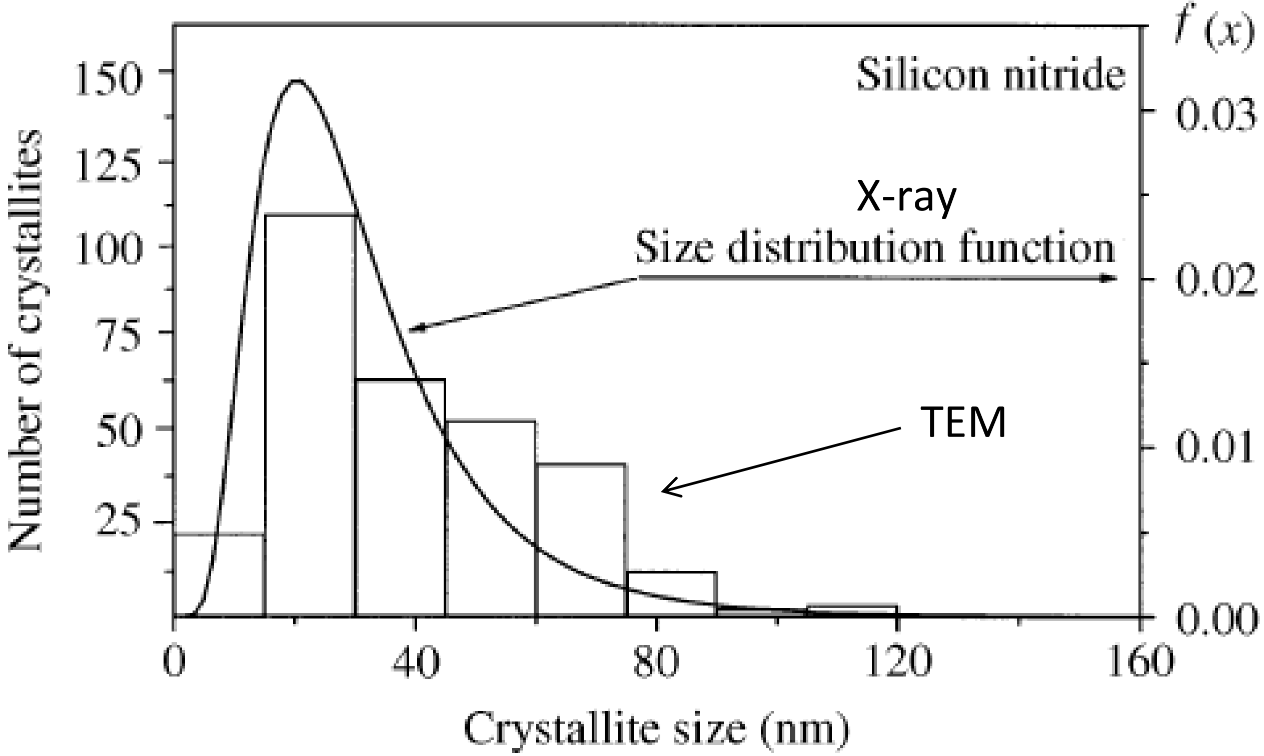

crystallite size (diffraction) ≈ particle size (TEM)

T. Ungár, J. Gubicza, G. Ribárik and A. Borbély, *J. Appl. Cryst.* (2001) **34**, 298-310.

Materials produced by significant amounts of plastic deformation

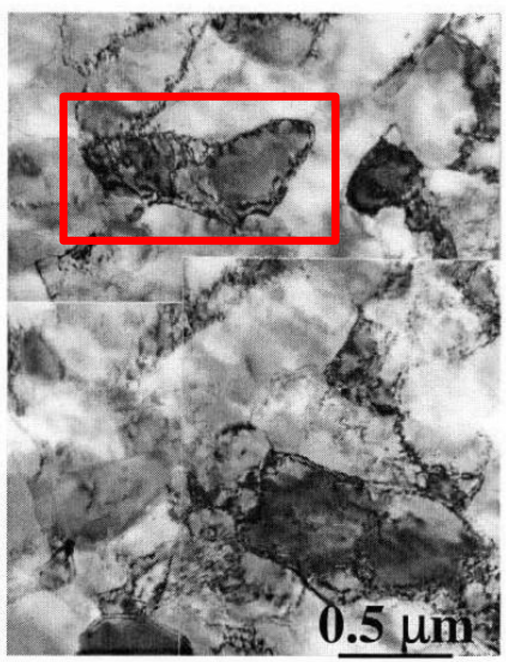

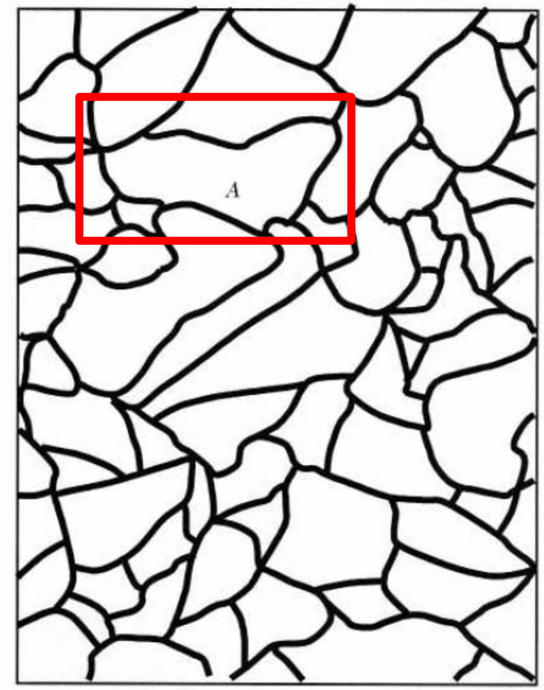

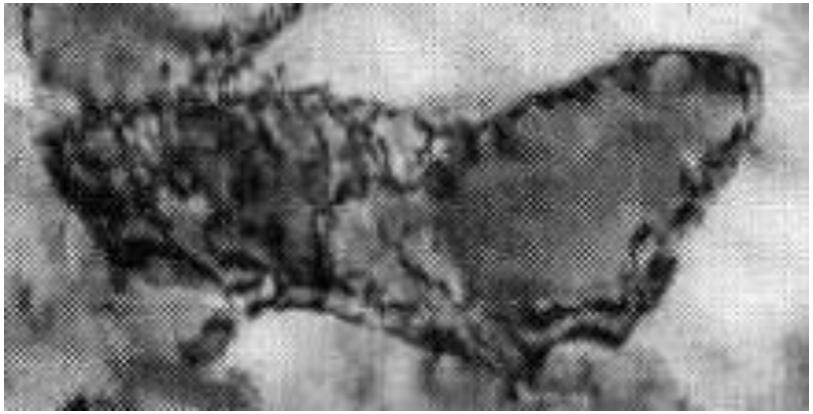

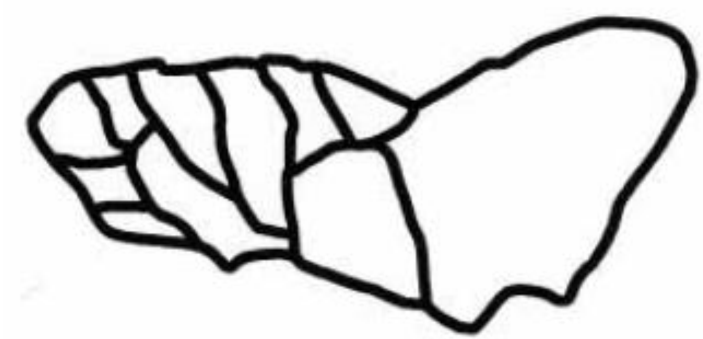

T. Ungár, J. Gubicza, G. Ribárik and A. Borbély, *J. Appl. Cryst.* (2001) **34**, 298-310.

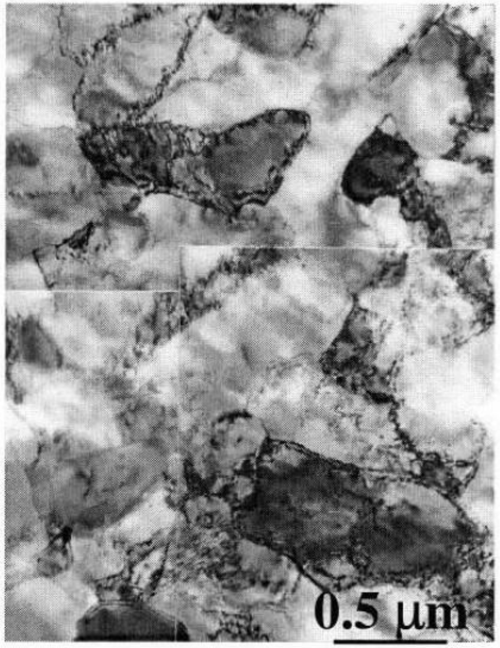

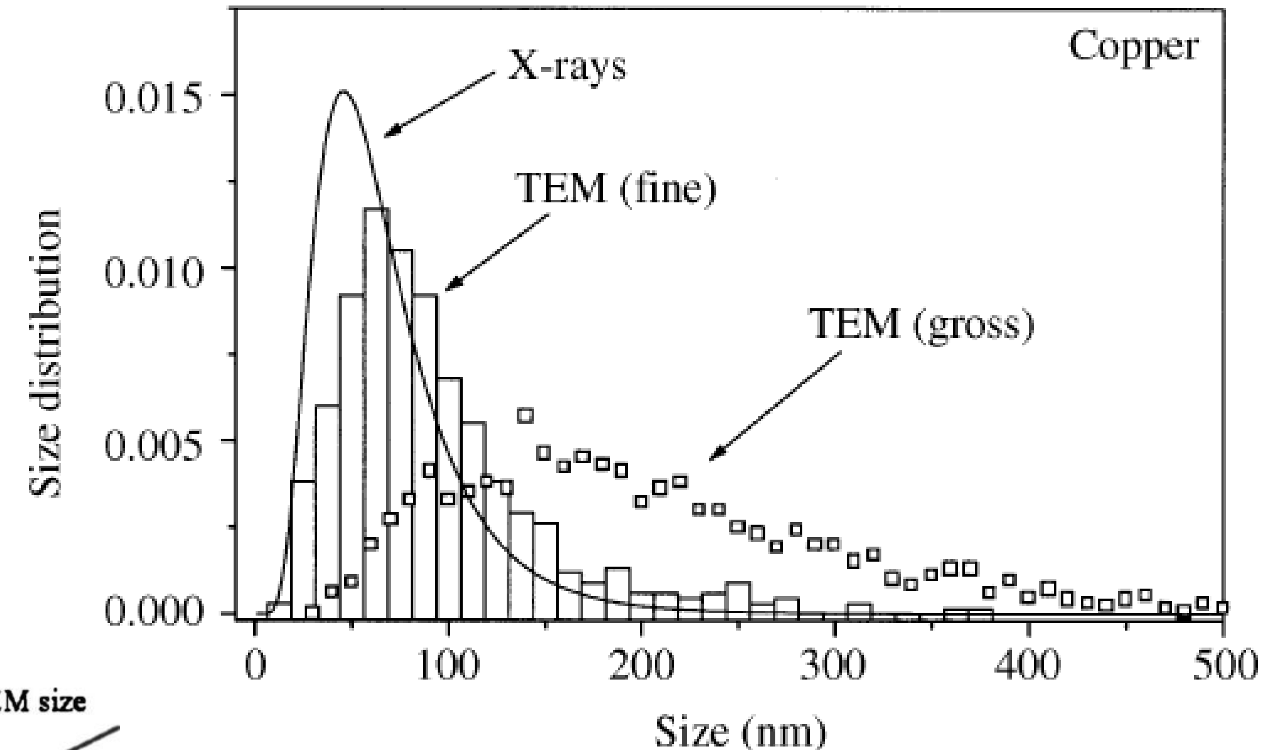

T. Ungár, J. Gubicza, G. Ribárik and A. Borbély, *J. Appl. Cryst.* (2001) **34**, 298-310.

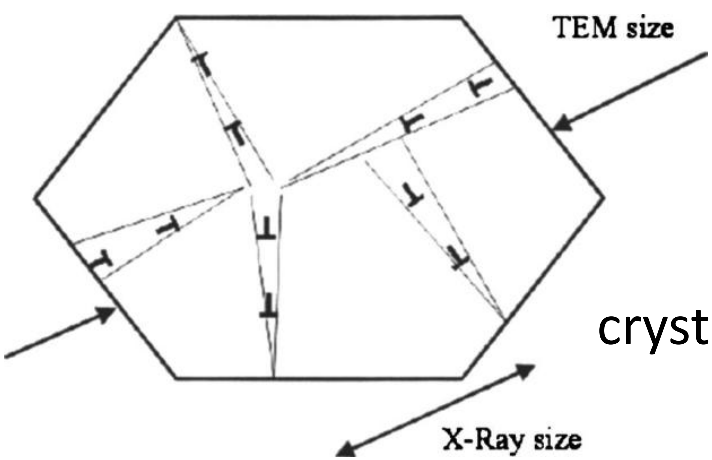

crystallite size (diffraction) ≈ cell/sub-grain size (TEM)

T. Ungár, G. Tichy, J. Gubicza, and R. Hellmig, *Powder Diff.* **20**, (2005) 366.

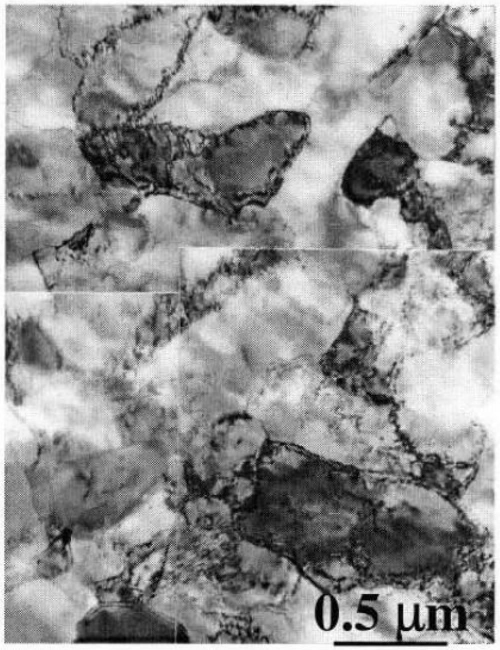

Maximum detectable average cell/sub-grain size by Diffraction Line Profile Analysis : ≅ **1 µm**

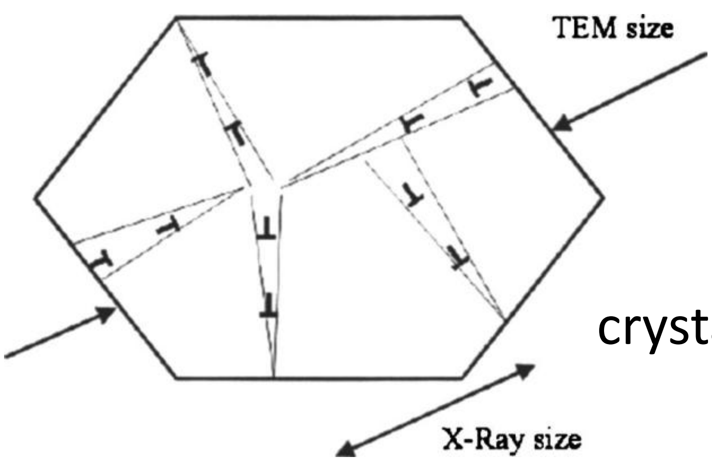

T. Ungár, J. Gubicza, G. Ribárik and A. Borbély, *J. Appl. Cryst.* (2001) **34**, 298-310.

crystallite size (diffraction) ≈ cell/sub-grain size (TEM)

T. Ungár, G. Tichy, J. Gubicza, and R. Hellmig, *Powder Diff.* **20**, (2005) 366.

Fundamental equation of line broadening

Warren & Averbach (1952):

$$A(L) = A_{size}(L) A_{pf}(L) \exp\left(-2\pi^2 g^2 L^2 \langle \varepsilon_{L,g}^2 \rangle\right)$$

Fourier transform of a broadened diffraction peak shape

Contribution of crystallite size distribution

Contribution of planar faults

The microstrain is characterized by the "mean square strain"

Contribution of the microstrain distribution found in the specimen

$< \varepsilon^2_{L,g} >$ for **dislocations** [Krivoglaz, Wilkens]:

Wilkens, M. (1970b). *Phys. Status Solidi A*, 2, 359±370.
Wilkens, M. (1987). *Phys. Status Solidi A*, 104, K1.
Krivoglaz, M. A. (1969). *Theory of X-ray and Thermal Neutron Scattering by Real Crystals.* New York: Plenum Press

$$\left\langle \varepsilon^2_{g,L} \right\rangle = \frac{\rho C b^2}{4\pi} f(\eta) \qquad \eta = \frac{L}{M\rho^{-0.5}}$$

$$E_{dens} \propto G b^2 \rho \ln\left(\frac{M\rho^{-0.5}}{r_0}\right)$$

ρ - Dislocation density

M - Dislocation arrangement

C - Dislocation contrast factor => Burgers vector types

Dislocation **arrangement** parameter

random | correlated, high dipole character

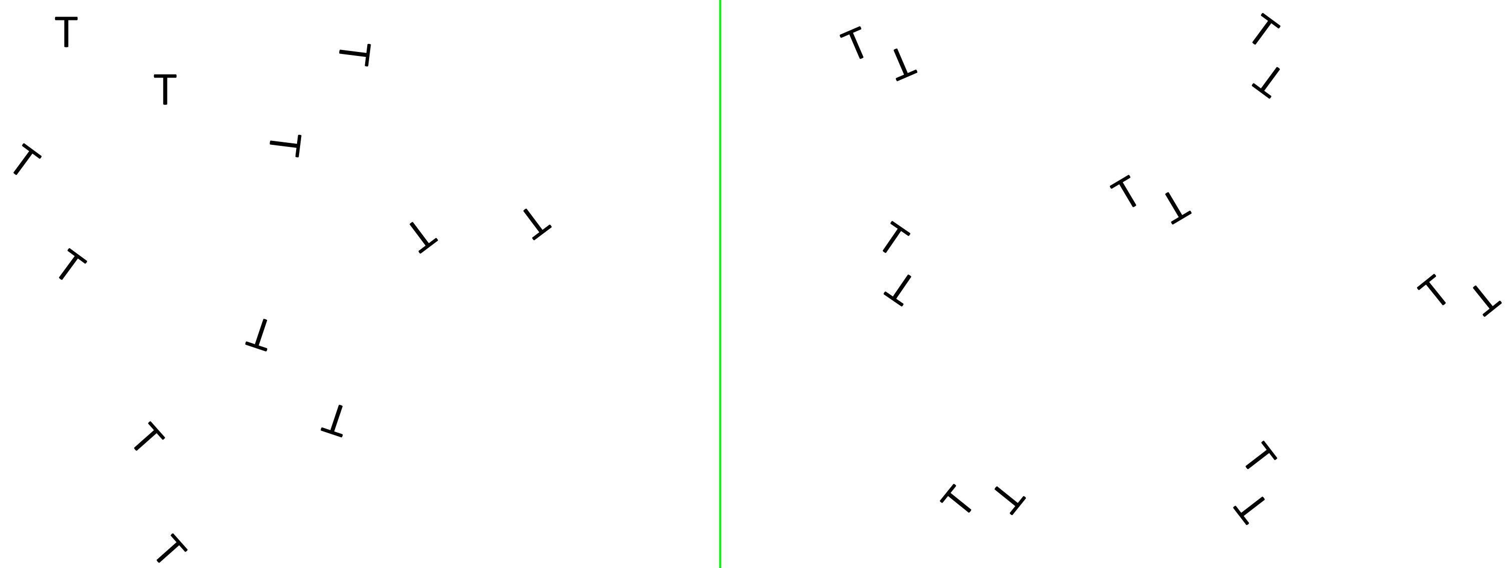

$$M_{rand} >> M_{corr}$$

E. Schafler, K. Simon, S. Bernstoff, P. Hanák, G. Tichy, T. Ungár & M. J. Zehetbauer, *Acta Mat.* **53** (2005) 315-322.

Knowing the FWHM of the profiles is not sufficient to determine ρ (and *M*) quantitatively, the full shape is needed

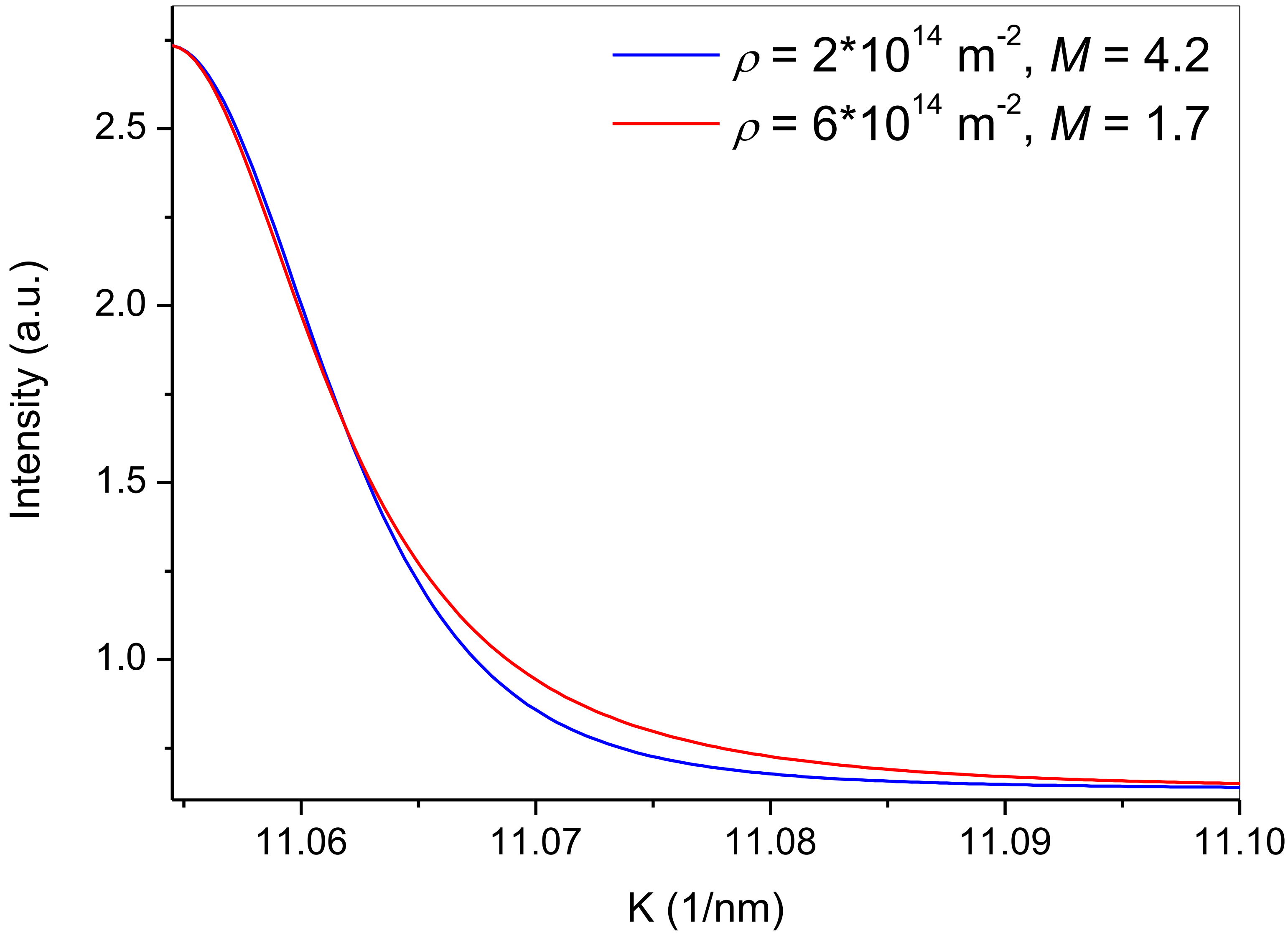

$< \varepsilon_{L,g}^2 >$ for **dislocations** [Krivoglaz, Wilkens]:

$$\left\langle \varepsilon_{g,L}^2 \right\rangle = \frac{\rho C b^2}{4\pi} f(\eta) \qquad \eta = \frac{L}{M \rho^{-0.5}}$$

C - Dislocation contrast factor

P. Klimanek & R. Kuzel *J. Appl. Cryst*. 21 (1988), 59-66.
T. Ungár & G. Tichy, *Phys. Status Solidi A*, 171 (1999) 425-434.
A. Borbély, I. C. Dragomir, G. Ribárik & T. Ungár, *J. Appl. Cryst.,* 36 (2003) 160-162.

The **dislocation contrast factor** carries information about the Burgers vector types present in the crystal

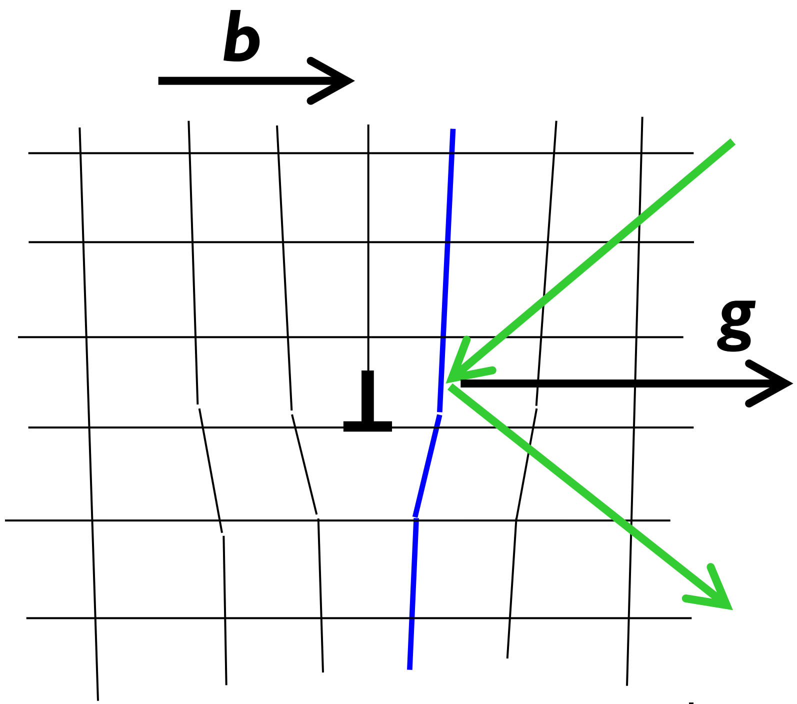

gb ≠ 0

dislocation is visible

strong contrast

strong line broadening

Images by: C. Nisr

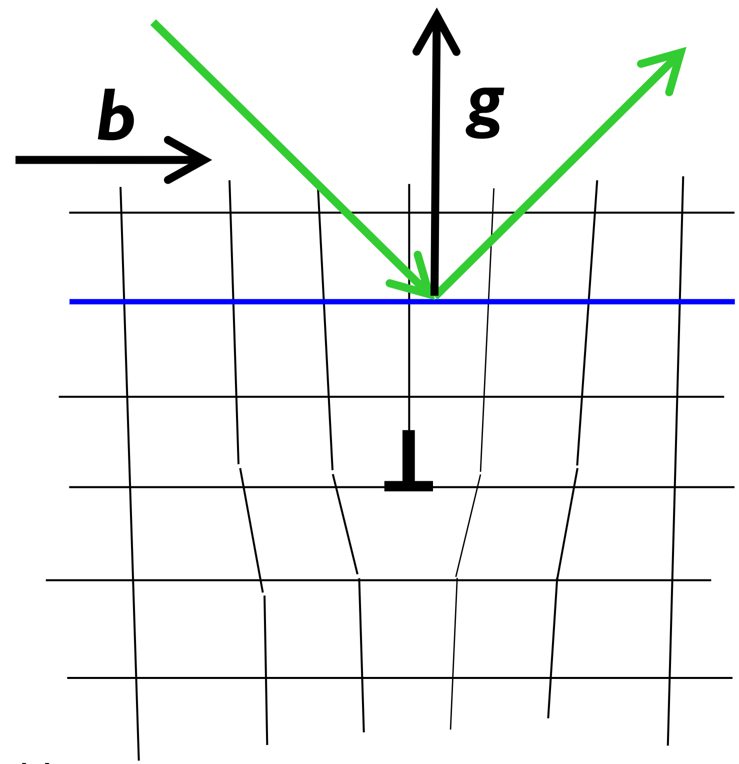

gb = 0

dislocation is invisible

weak contrast

weak line broadening

Dislocation contrast in TEM

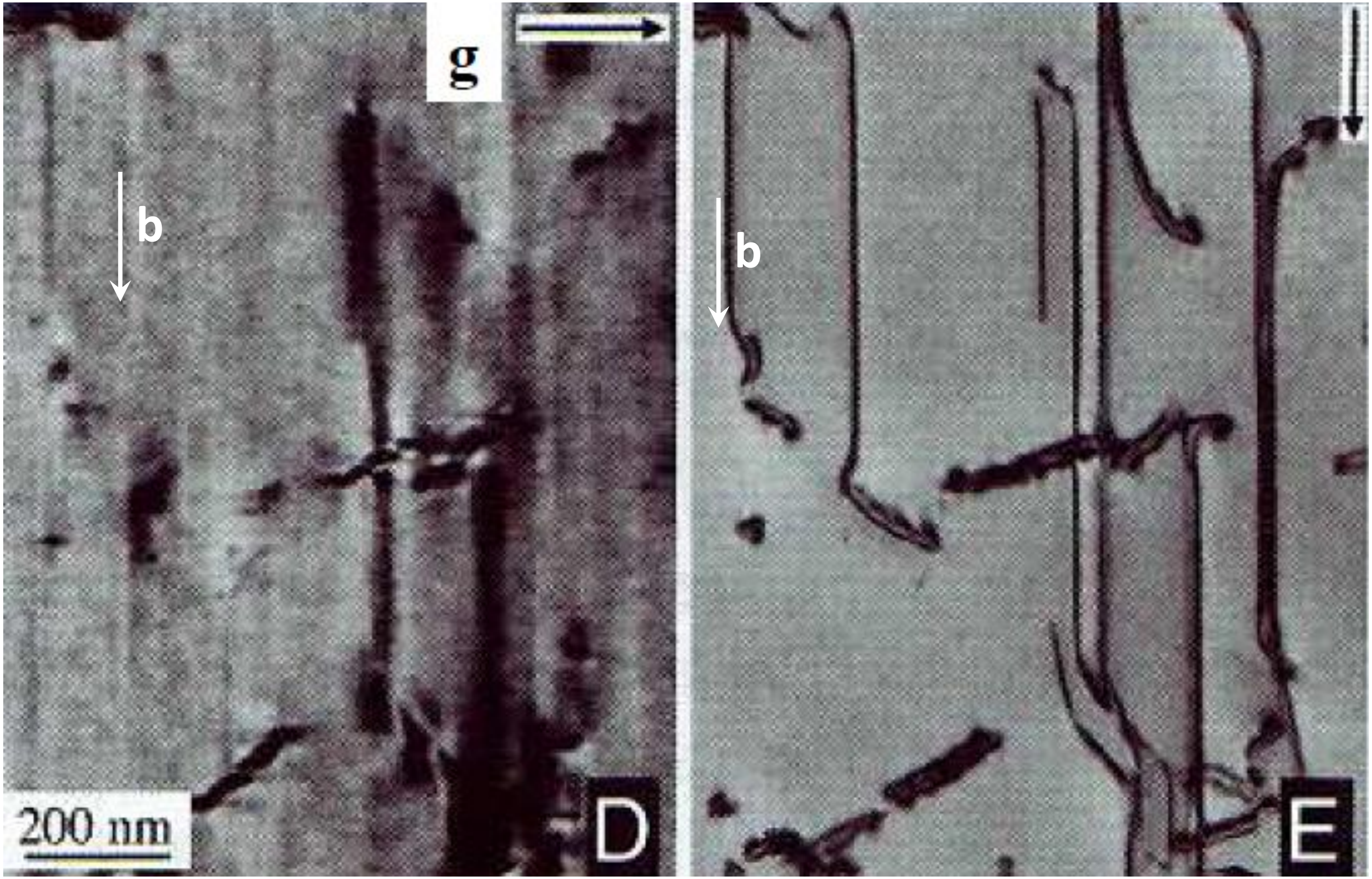

Ni_3Al foil

B. D. Williams, C. B. Carter, *Transmission Electron Microscopy*, 1996 Plenum Press, New York

Detection limits of Diffraction Line Profile Analysis

average distance between dislocations: $\bar{D}_{disloc} = \frac{1}{\sqrt{\rho}}$

$\bar{D}_{disloc} \cong 1\mu m$ ⟷ $\rho_{min} \cong 10^{12} - 10^{13} m^{-2}$

Minimum detectable dislocation density by Diffraction Line Profile Analysis is in the range of: ≅ $\mathbf{10^{13}\ m^{-2}}$

Fundamental equation of line broadening

Warren & Averbach (1952):

$$A(L) = A_{size}(L)\,A_{pf}(L)\,\exp\left(-2\pi^2 g^2 L^2 \langle \varepsilon_{L,g}^2 \rangle\right)$$

Fourier transform of a broadened diffraction peak shape

Contribution of crystallite size distribution

Contribution of planar faults

Contribution of the microstrain distribution found in the specimen

Planar Defects: twinning and stacking faults

fcc

fcc sequence	Intrinsic SF	Extrinsic SF	Twins
C	*A*	*B*	*C*
B	*C*	*A*	*A*
A	*B*	*B*	*B*
C	*C*	*C*	*C*
B	*B*	*B*	*B*
A	*A*	*A*	*A*

hcp

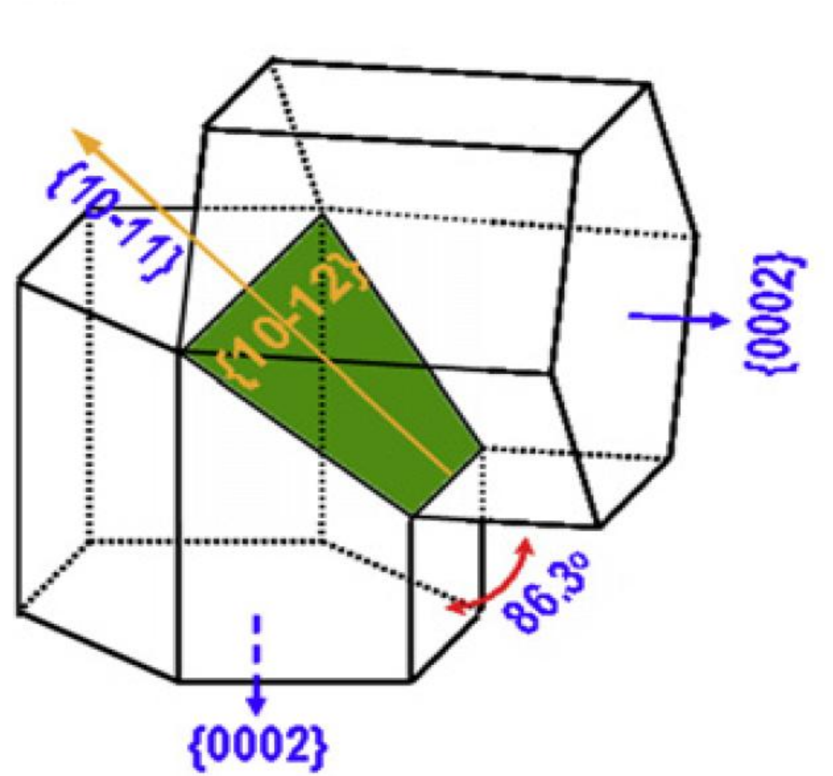

L. Wu, A. Jain, D.W. Brown, G.M. Stoica, S.R. Agnew, B. Clausen, D.E. Fielden, P.K. Liaw Acta Materialia 56 (2008) 688–695

Streaking: Twins in nanocrystalline NiTi

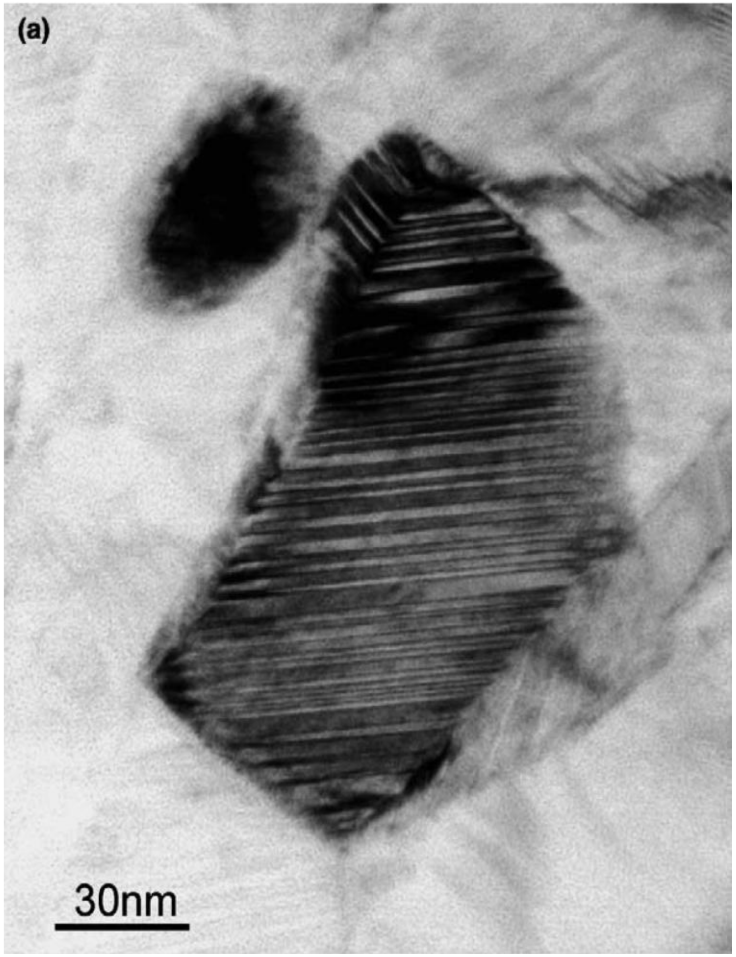

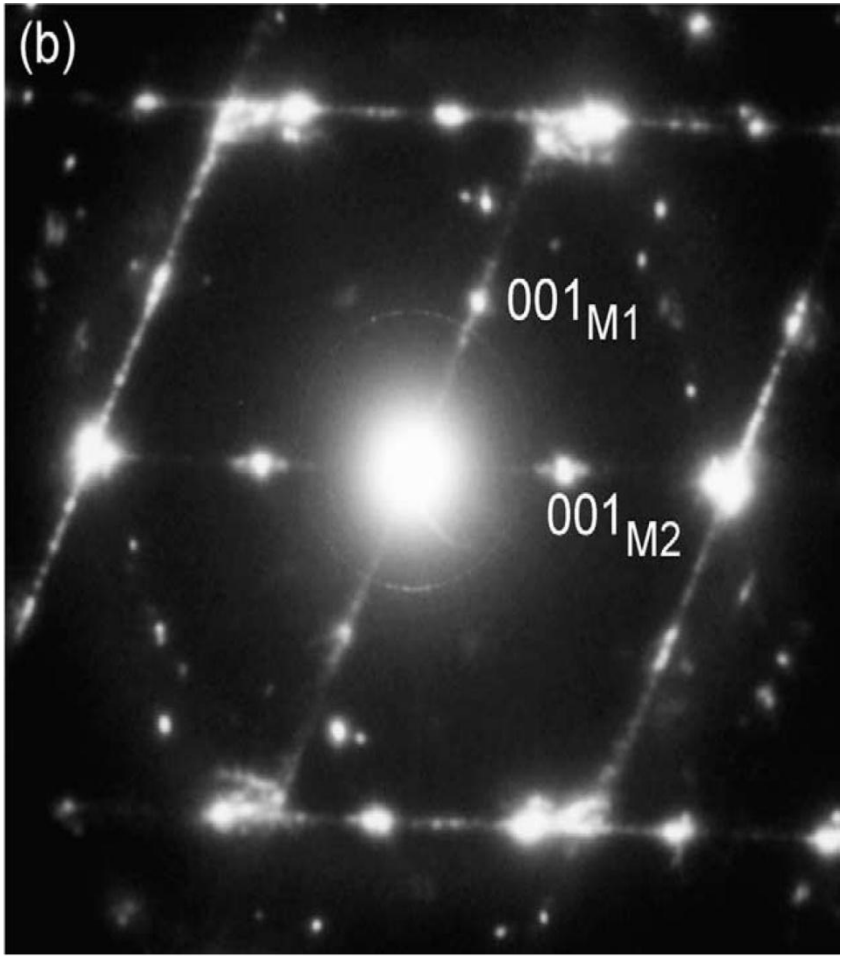

T. Waitz, V. Kazykhanov, H.P. Karnthaler, Acta Materialia 52 (2004) 137–147

Streaking: Planar Defects in Magnesium-Fluorogermanate

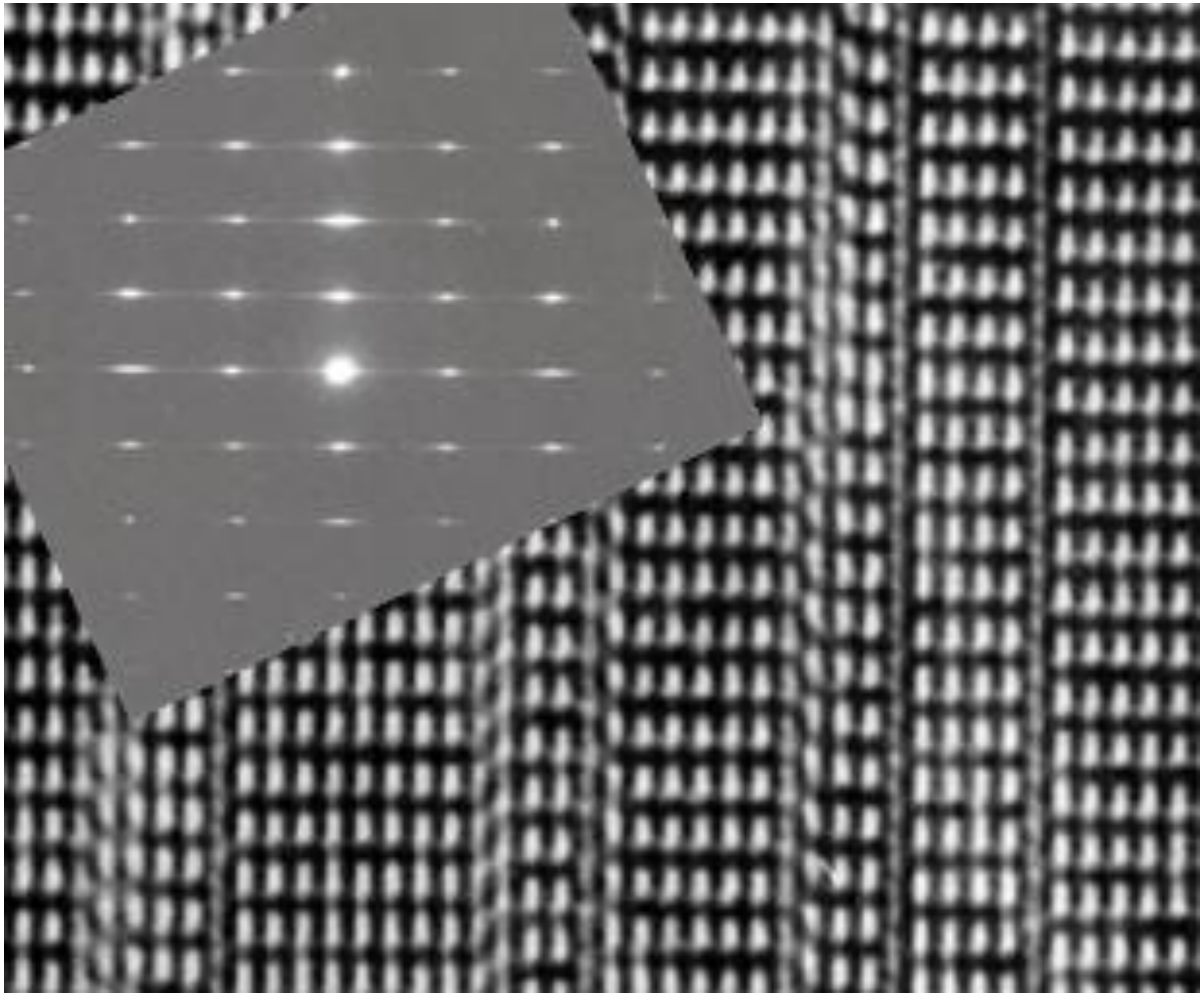

P. Kunzmann in J.M. Cowley, Acta Cryst. (1976). A32, 83

Integrating the streak profiles to obtain powder patterns

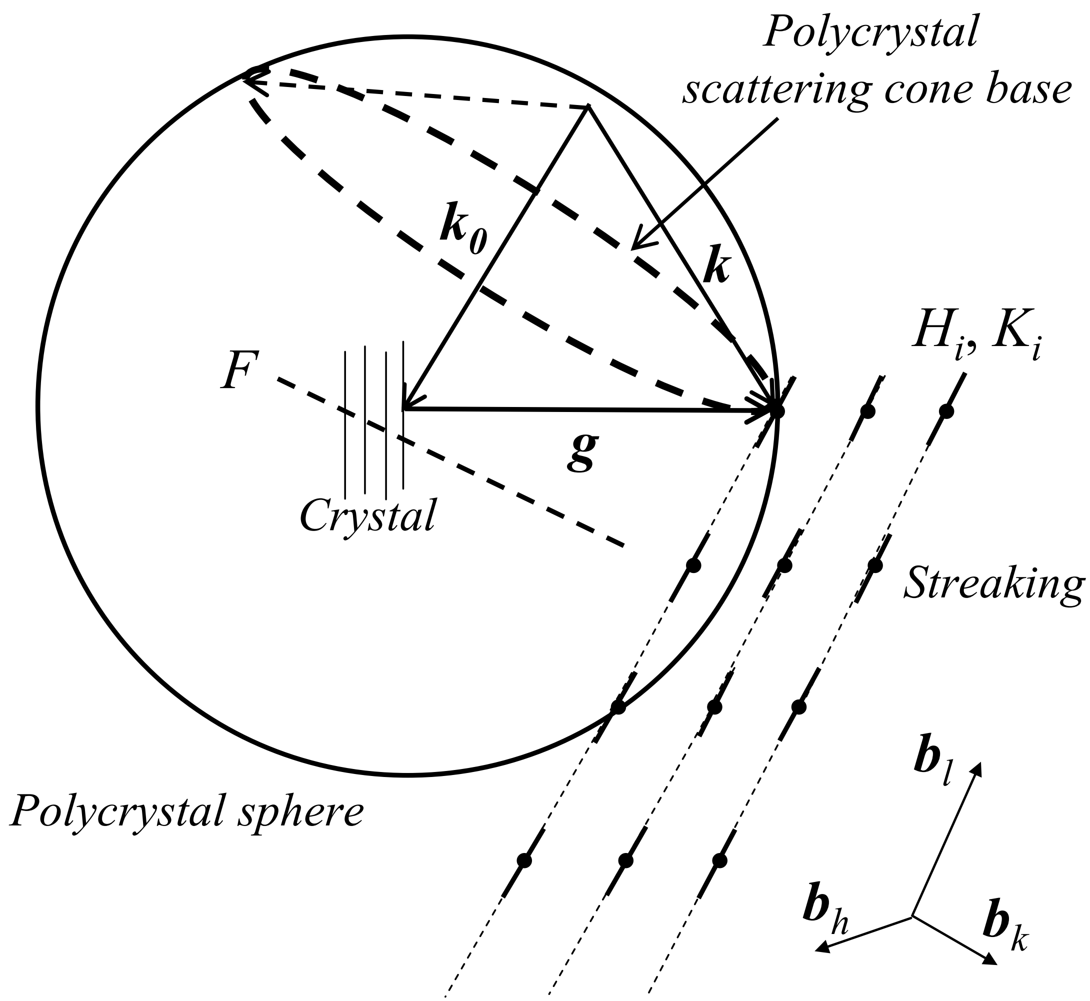

L. Balogh, G. Tichy and T. Ungár *J. Appl. Cryst. 42, (2009)* 580-591.

Powder profiles → weighted sum of differentely broadened *sub-reflections*

{11.4} powder diffraction profile

Twinning on {10.2} planes

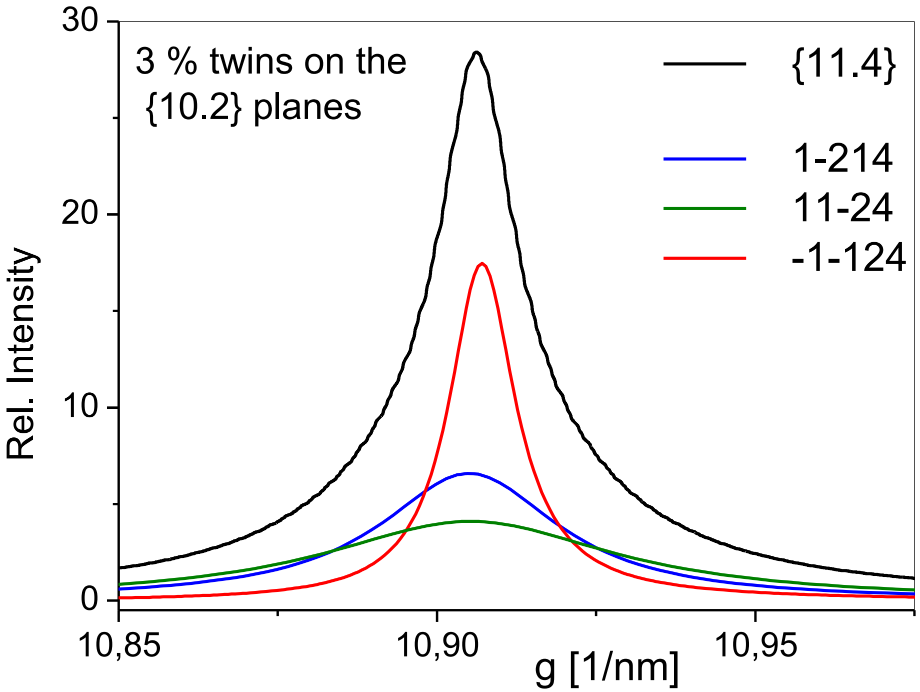

Twinning on {10.1} planes

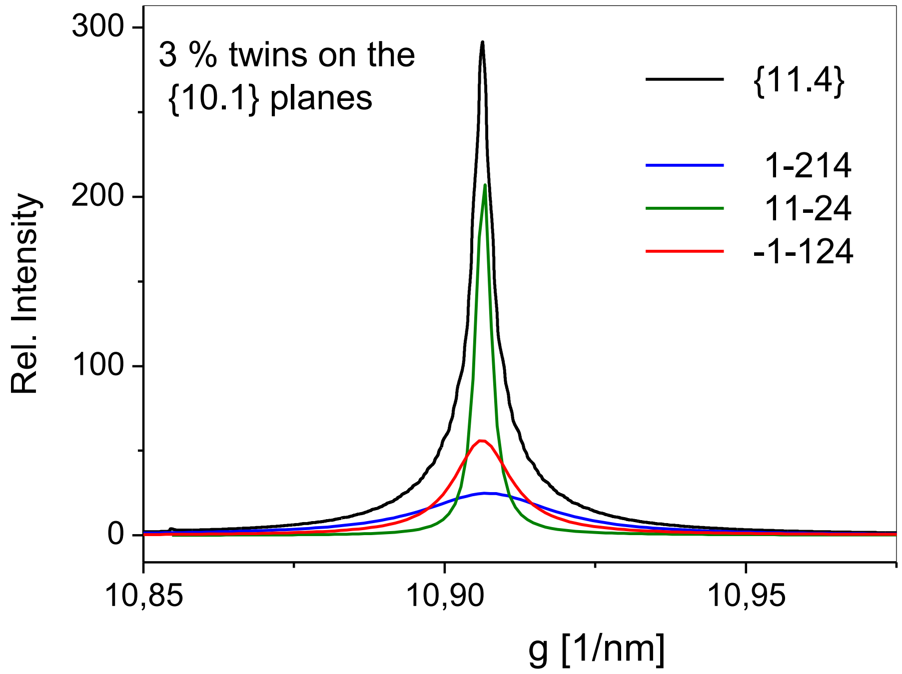

L. Balogh, G. Tichy and T. Ungár *J. Appl. Cryst. 42, (2009)* 580-591.

nano-SiC sintered at 2 Gpa and 1800 °C

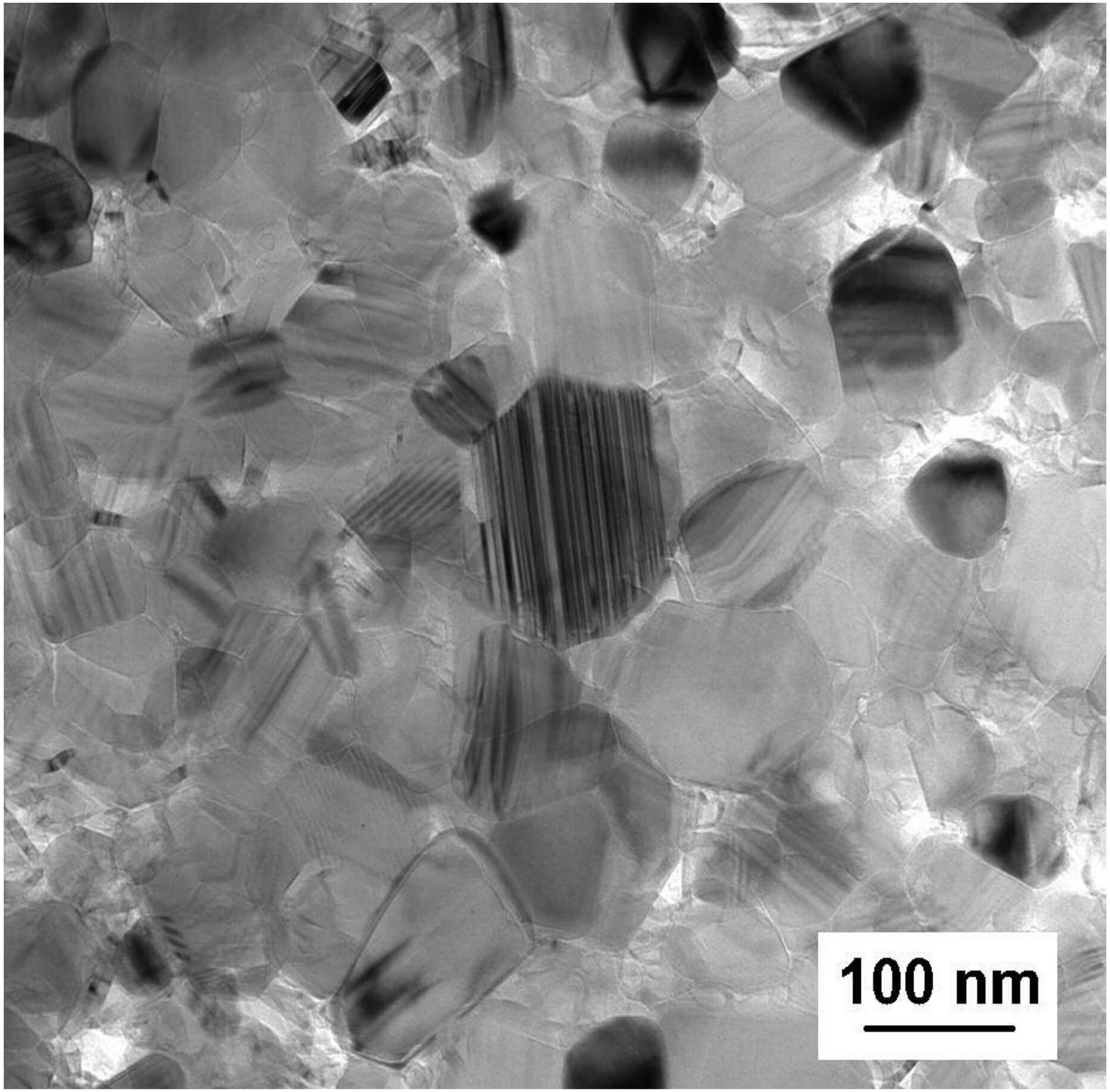

$$\bar{D}_{twin} \cong 23 \pm 3\, nm$$

J. Gubicza, S. Nauyoks, L. Balogh, J. Lábár, T. W. Zerda, T. Ungár, *J. Mater. Res.* **22** (2007) 1314

Detection limits of Diffraction Line Profile Analysis

average distance between twin boundaries:

$$\overline{D}_{twin} = \frac{1}{\beta} d_T, \qquad d_T \cong 0.1 - 0.2\, nm$$

$$\overline{D}_{twin} \cong 1\mu m \quad \longleftrightarrow \quad \beta \cong 0.02\%$$

Minimum detectable twin boundary frequency by Diffraction Line Profile Analysis is in the range of: ≅ ***0.02 %***

Data quality requirements

Diffraction Line Profile Analysis needs high angular resolution and good statistics

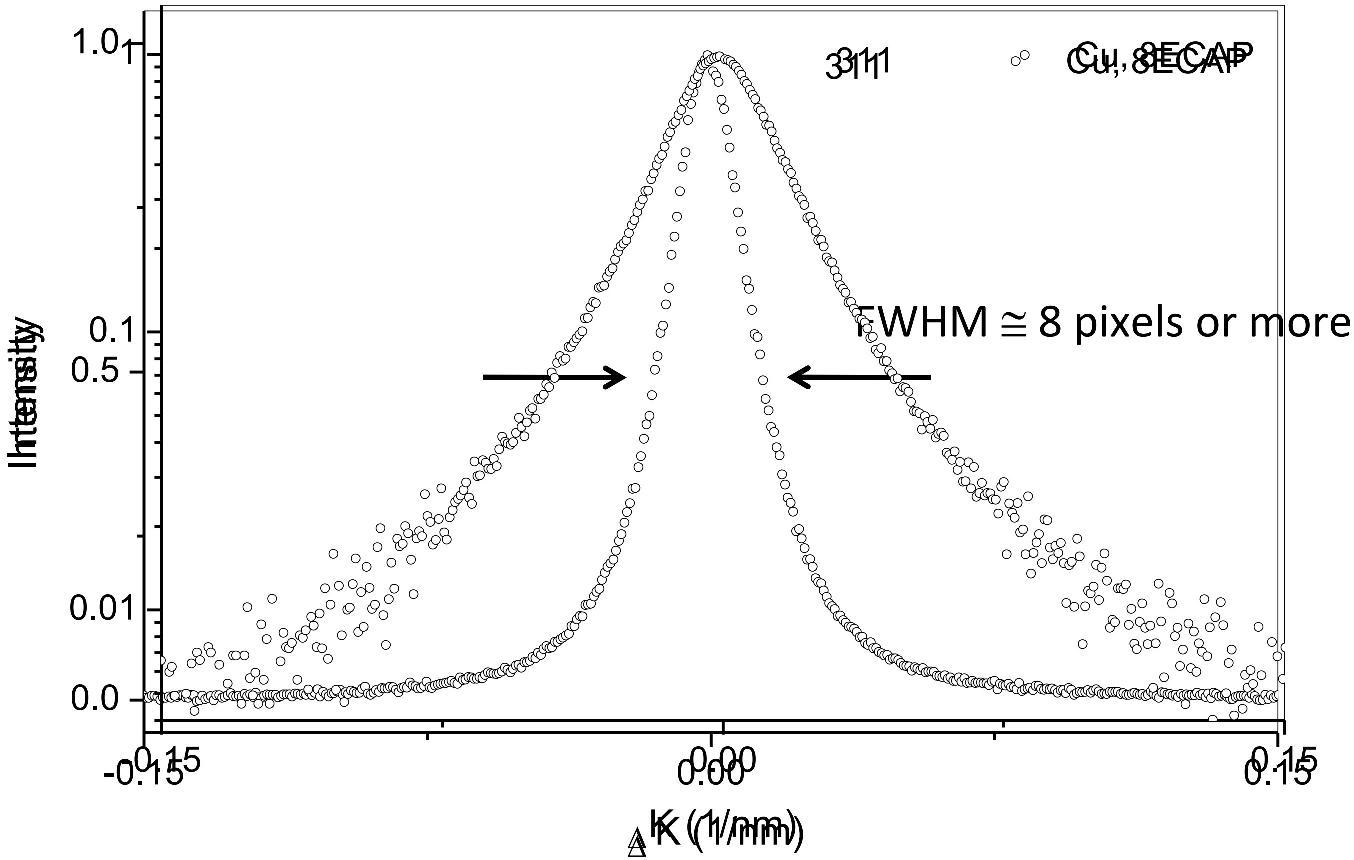

$K = 1/d$, $\Delta K = K - K_0$

- good statistics: 5000-6000 or more counts in the bin of the peak maxima

- the whole diffraction pattern is modeled using *theoretical profile functions based on fundamental physical principles* applied to the different microstructural characteristics

- Scardi & Leoni (2002): **Whole Powder Pattern Modeling (WPPM)**
  P. Scardi & M. Leoni, *Acta Cryst.* A58 (2002) 190-200.

- Ungár & Ribárik (2004): **extended Convolutional Multiple Whole Profile (eCMWP)**
  Ungár T., Gubicza J., Ribárik G., Borbély A.; *J Appl Cryst.* 34 (2001) 298–310
  G. Ribárik, J. Gubicza & T. Ungár, *Mat. Sci. Eng. A* 387-389 (2004) 343-347.

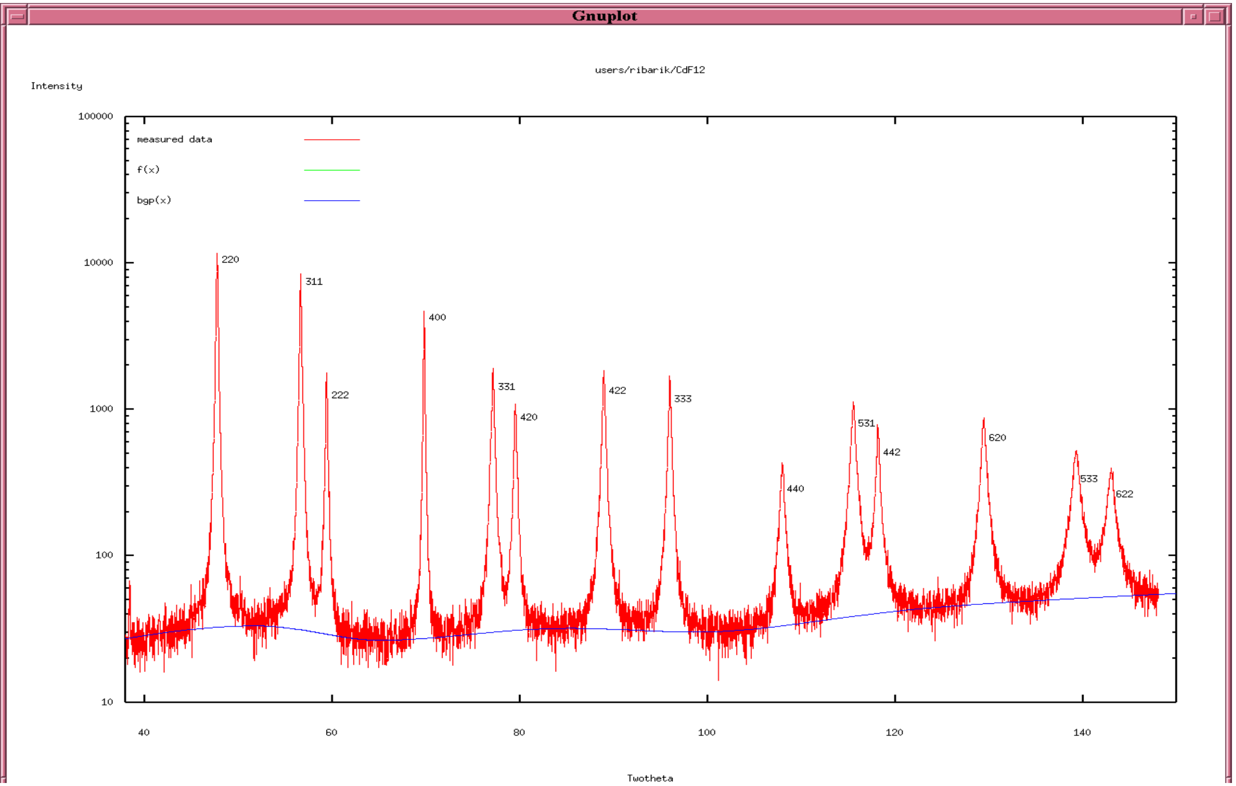

G. Ribárik, N. Audebrand, H. Palancher, T. Ungár and D. Louër, *J. Appl. Cryst.* (2005). 38, 912–926

The quantitative microstructure evaluation is performed using:

eCMWP (extended Convolutional Multiple Whole Profile) method

$$I_{Meas} <=> I_{Strain} * I_{Size} * I_{PlanarFault} * I_{Instr} + BG$$

Measured pattern — *Physically modeled* — *Experimentally determined*

Ungár T., Borbély A. *Appl. Phys. Lett. 69 (1996) 3173-3175.*

Ungár T., Tichy G. *Phys. Status Solidi A 171 (1999) 425-434.*

Ungár T., Gubicza J., Ribárik G., Borbély A. *Journal of Applied Crystallography 34 (2001) 298.*

Ribárik G., Gubicza J., Ungár T., *Mat. Sci. Eng. A* 387-389 (2004) 343-347.

Ribárik G., Jóni J., Ungár T., *J. Mater. Sci. & Tech. 35* (2019) 1508-1514.

Example 1: irradiated Zr-2.5Nb alloy

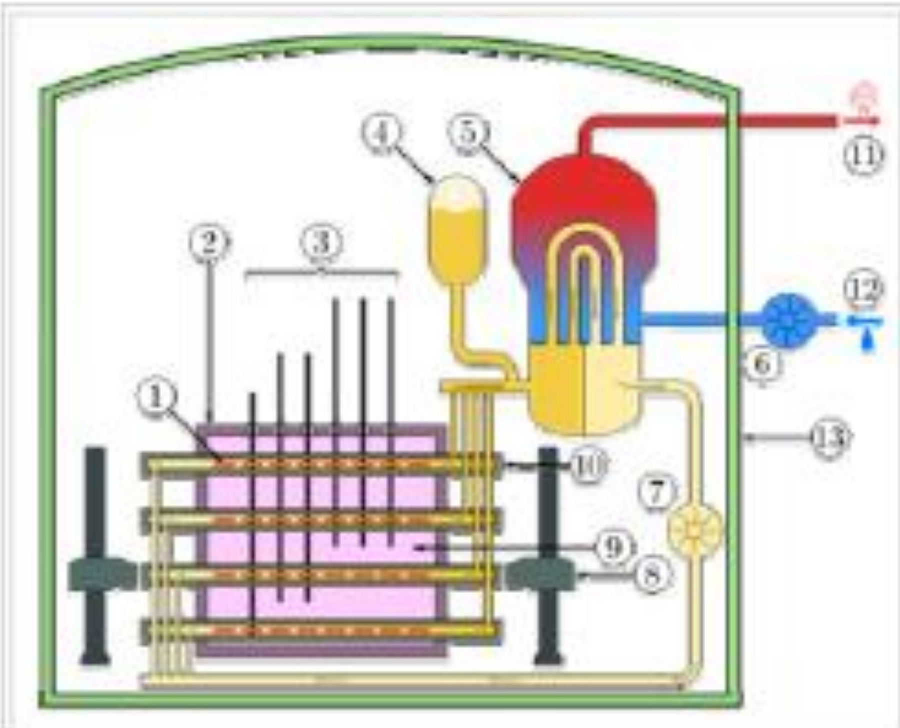

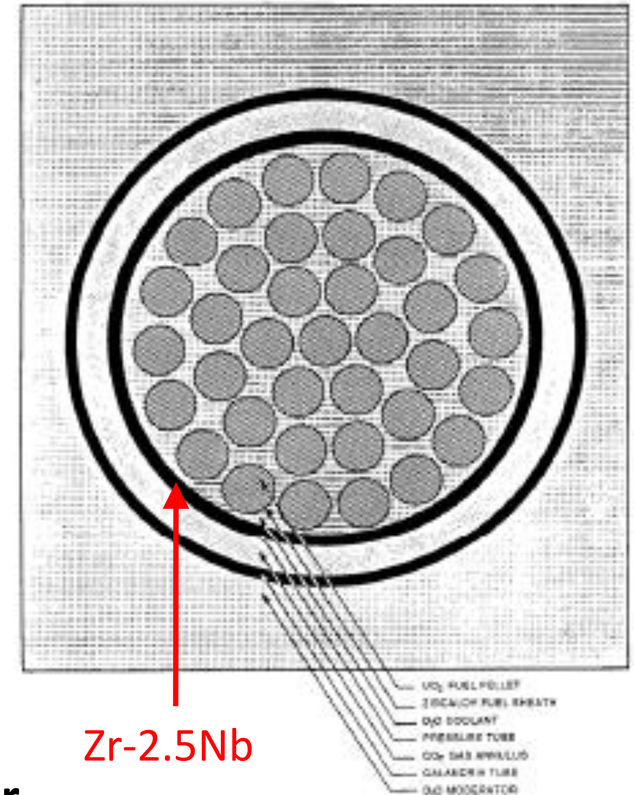

CANDU Basic Lattice Cell for 37-Element Fuel (Not to Scale)

- Removed from pressure tubes in a CANDU reactor.
  - Cold worked prior to service.
  - 7 years of service.
  - 250C, close to the cooling water inlet.
  - Neutron fluence $1.6x10^{24}/m^2$.

Samples provided by:
Nuclear Materials Research Group,
Queen's University, Kingston, ON, Canada
Chalk River Laboratories,
Atomic Energy Canada Ltd., Canada

The samples for annealing are cut from the irradiated Zr-2.5Nb pressure tube

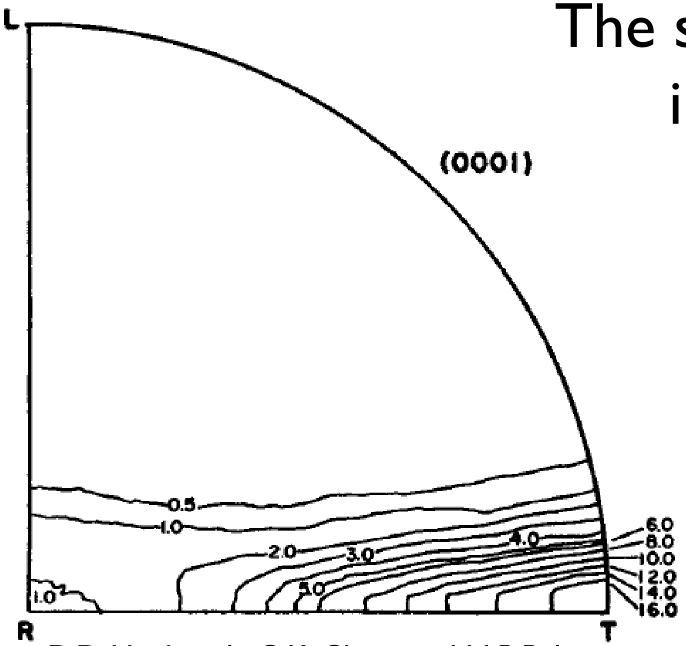

D.D. Himbeault, C.K. Chow, and M.P. Puls, Met. Mat. Trans. A, (1994) 25A 135-145.

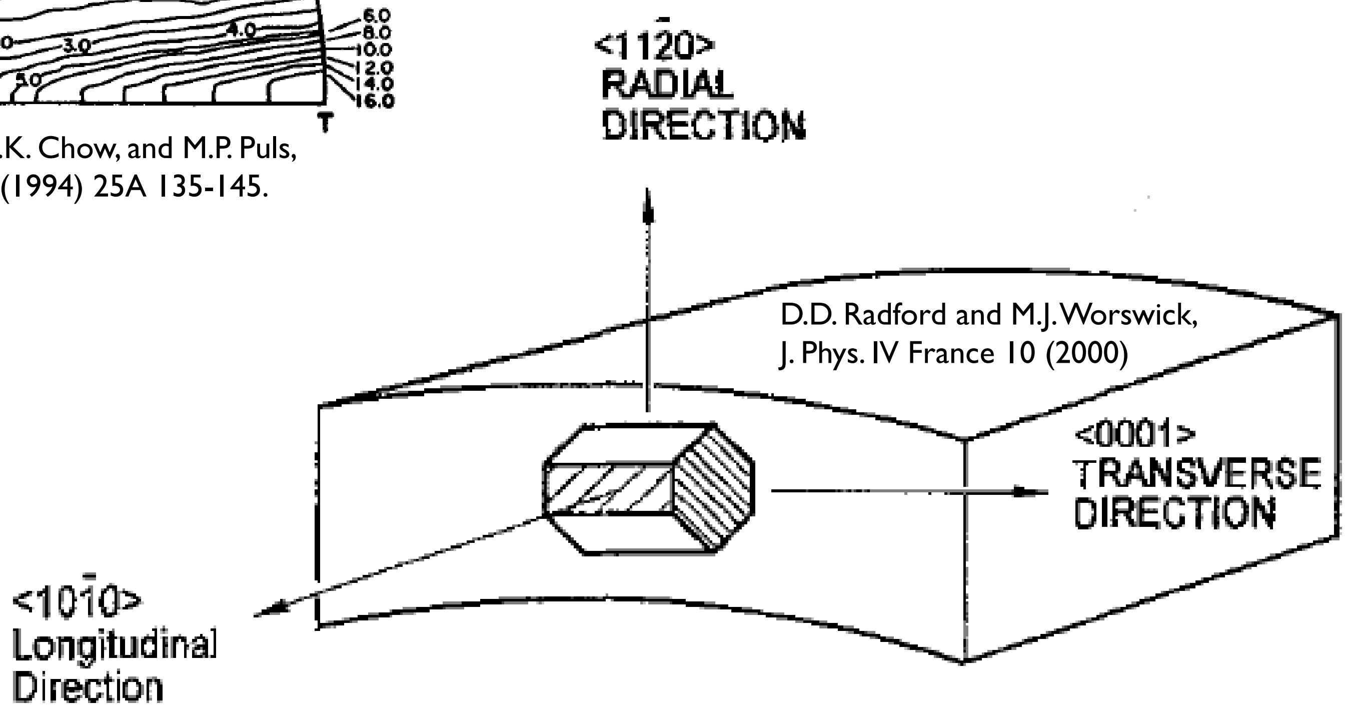

D.D. Radford and M.J. Worswick, J. Phys. IV France 10 (2000)

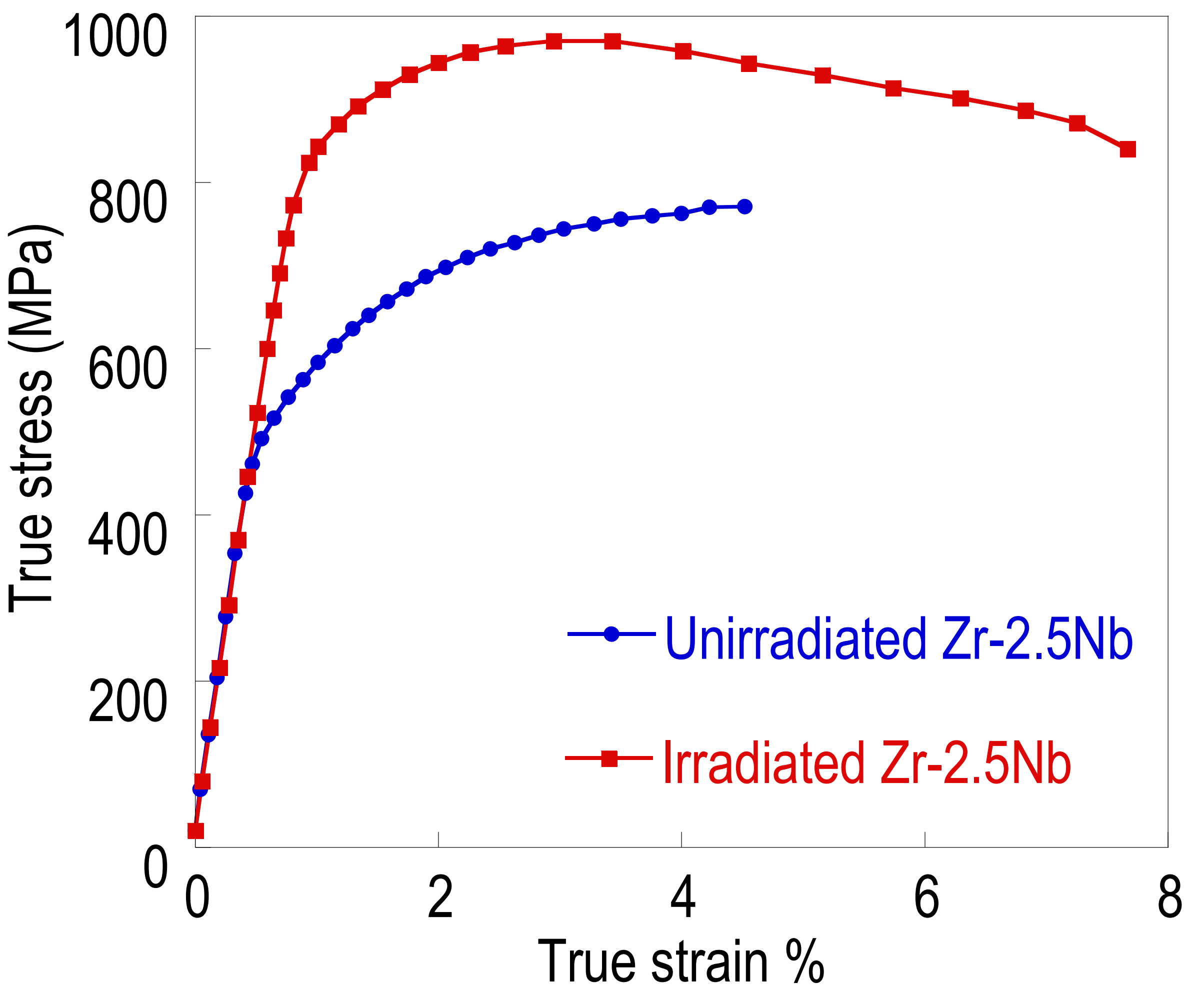

- the tensile direction was parallel with the longitudinal direction of the pressure tube

Sample	Yield strength
Un-irradiated Longitudinal(UL)	527MPa
Irradiated Longitudinal(IL)	824MPa

High resolution time-of-flight neutron diffraction measurements performed at the Neutron Powder Diffractometer (NPDF), Lujan Neutron Scattering Center, LANL

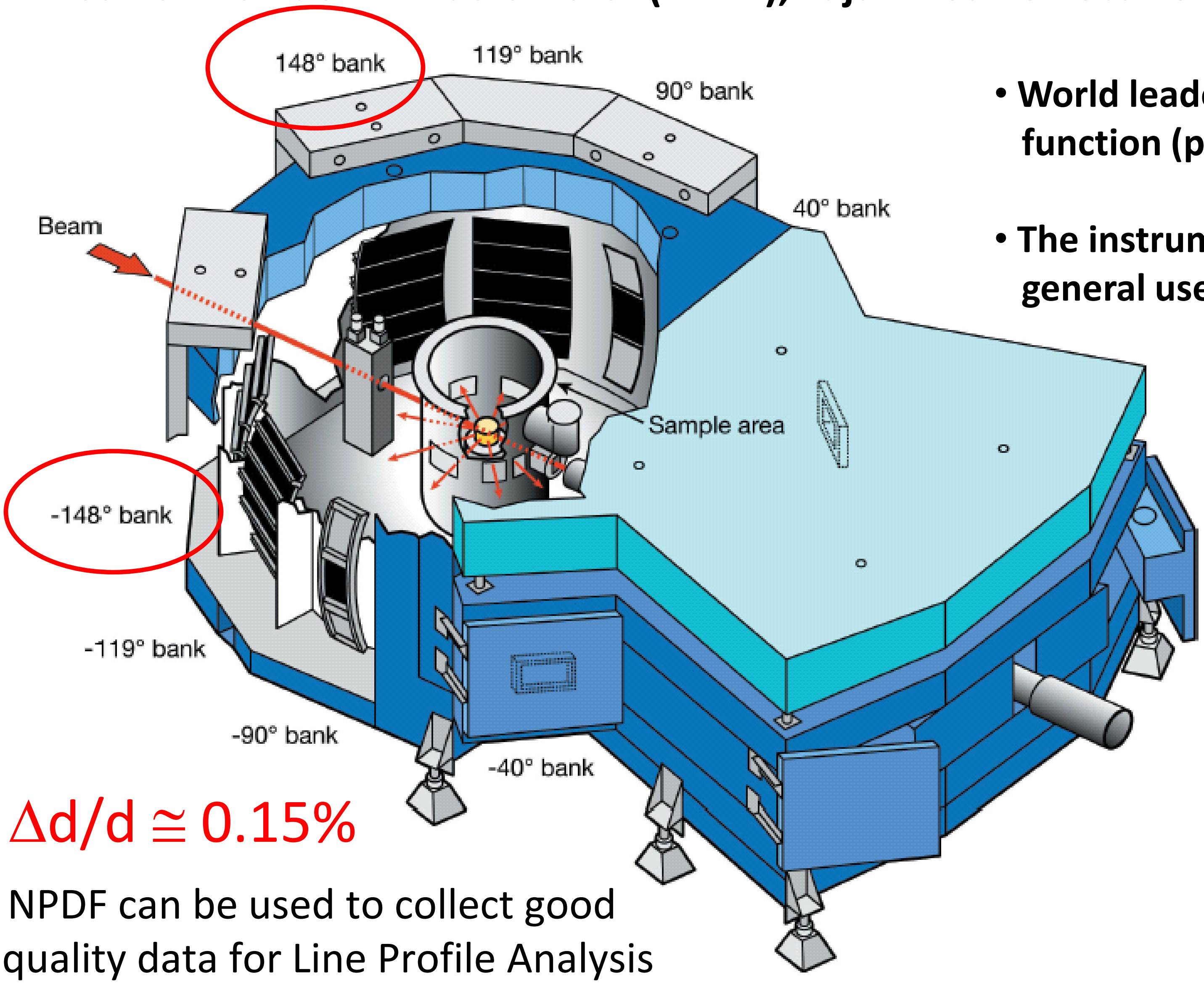

- **World leader in pair distribution function (pdf) studies**
- **The instrument is available to general users**

$\Delta d/d \cong 0.15\%$

- NPDF can be used to collect good quality data for Line Profile Analysis

Significant line profile broadening is observed, which is strongly hk.l dependent

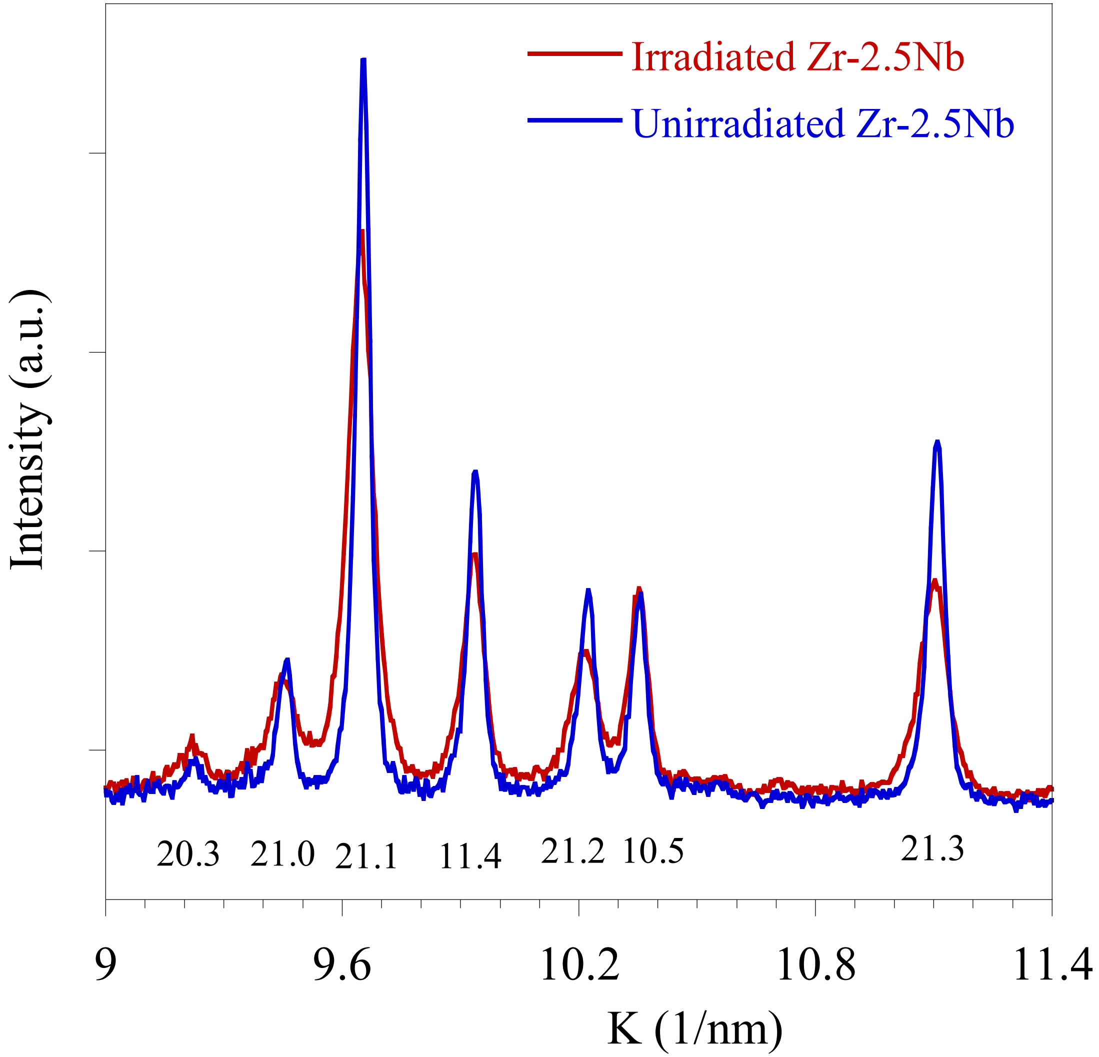

Significant line profile broadening is observed, which is strongly hk.l dependent

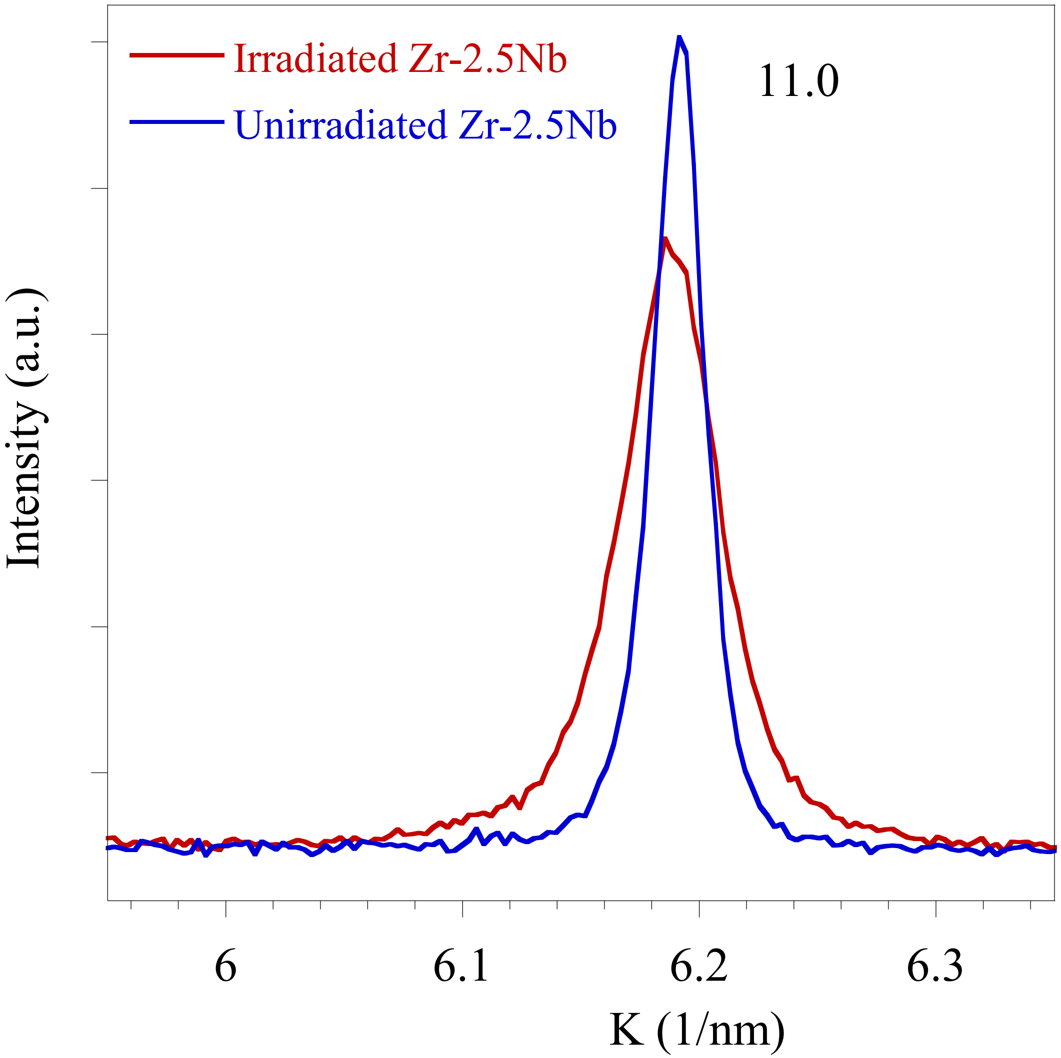

Qualitative assesments based on the peak width changes due to irradiation

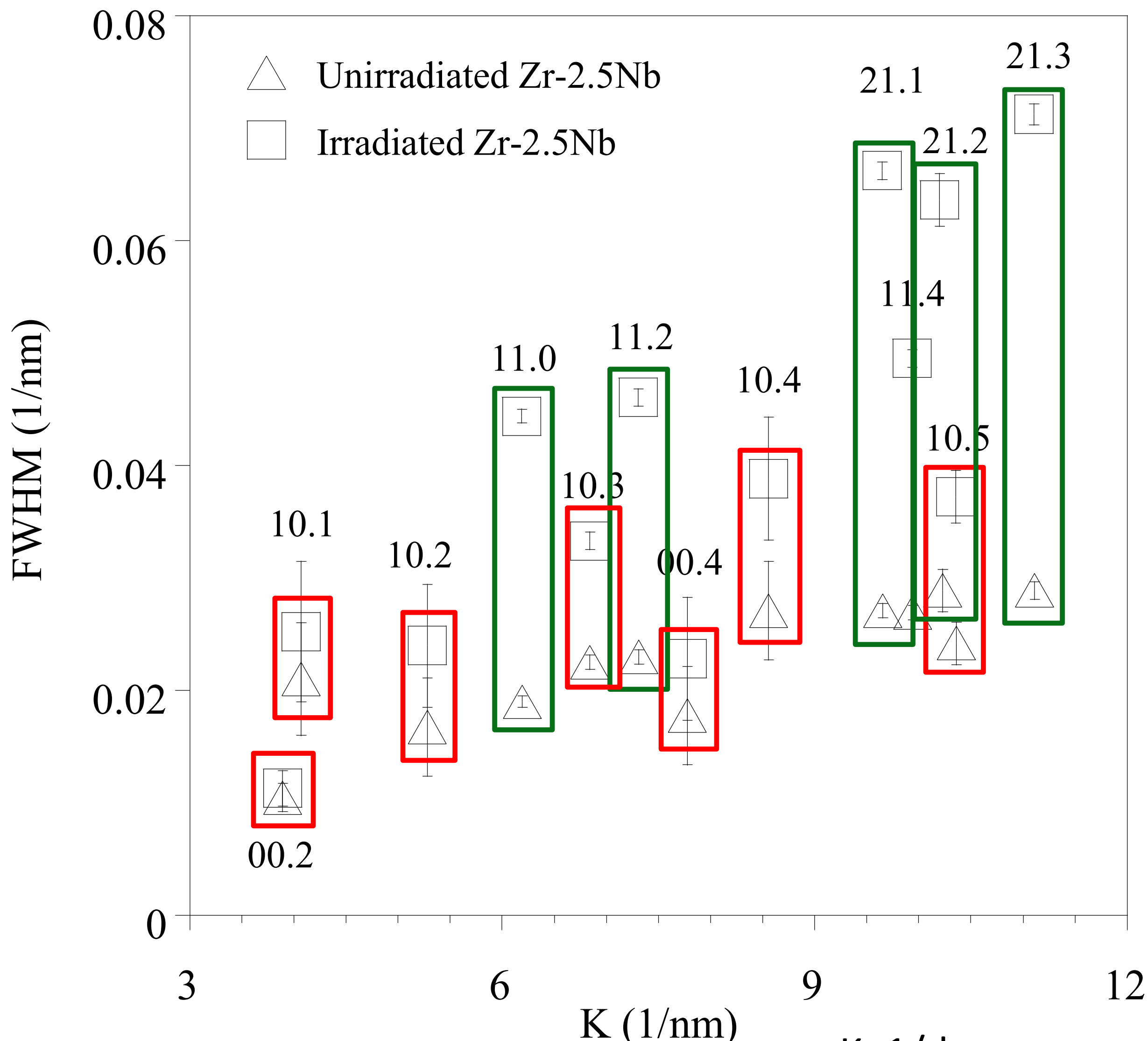

K=1/d

small FWHM change =>

gb ≅ 0

00.2, 00.4, 10.4, 10.5,10.3

large FWHM change =>

gb ≠ 0

11.0, 11.2, 21.1, 21.3,21.2

Irradiation creates mainly <a> Burgers vectors?

The effect of the **dislocation contrast factors** in TEM

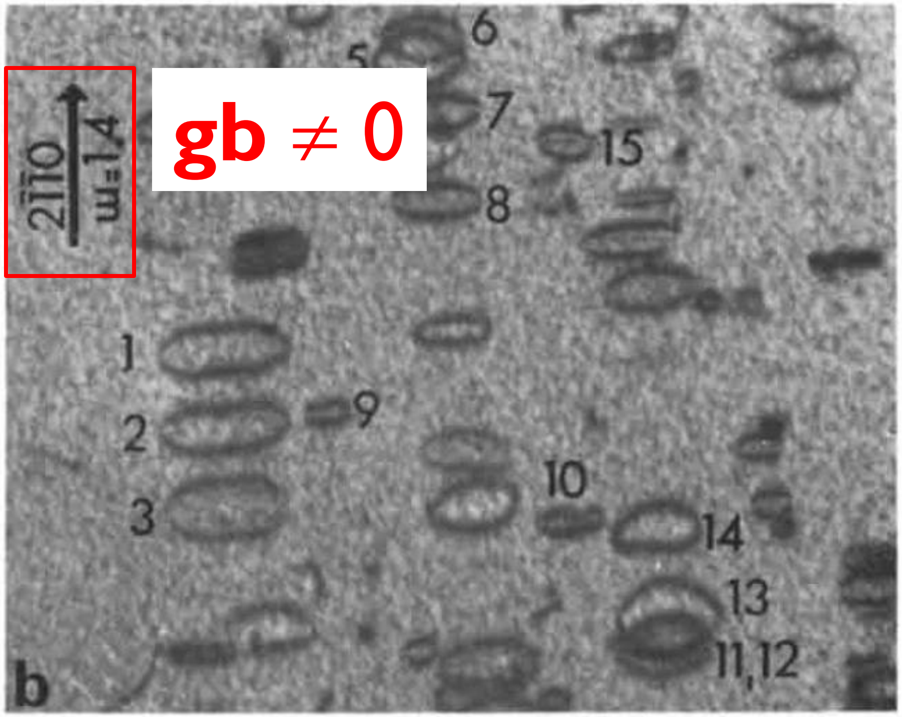

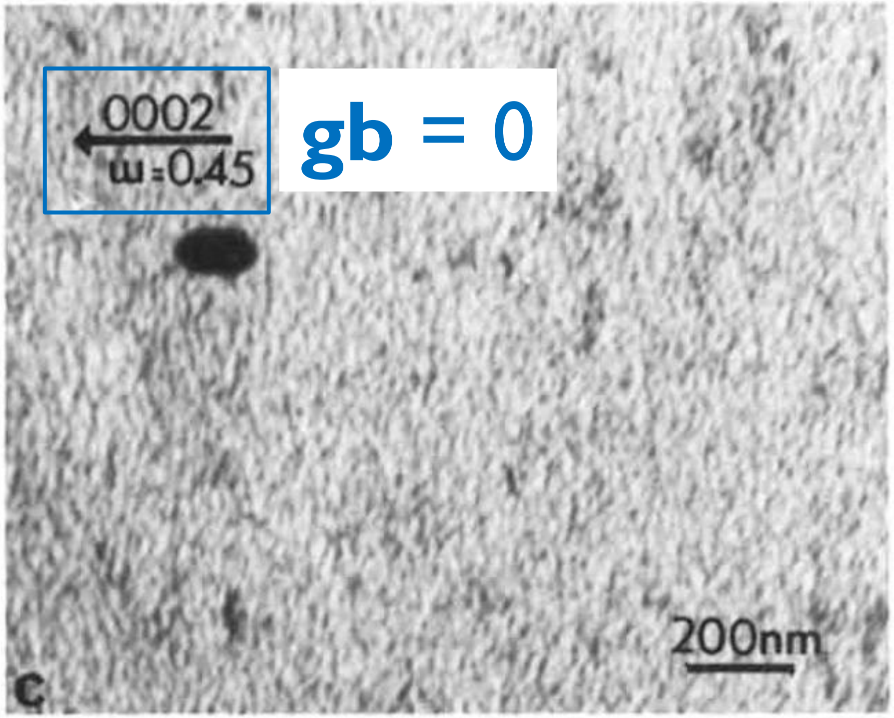

Jostsons, A., Kelly, P. M. and Blake, R. G., *Journal of Nuclear Materials*, **66** (1977) 236-256.

Quantitative dislocation densities obtained by the eCMWP method: the microstructure of the pre-annealed irradiated Zr-2.5Nb

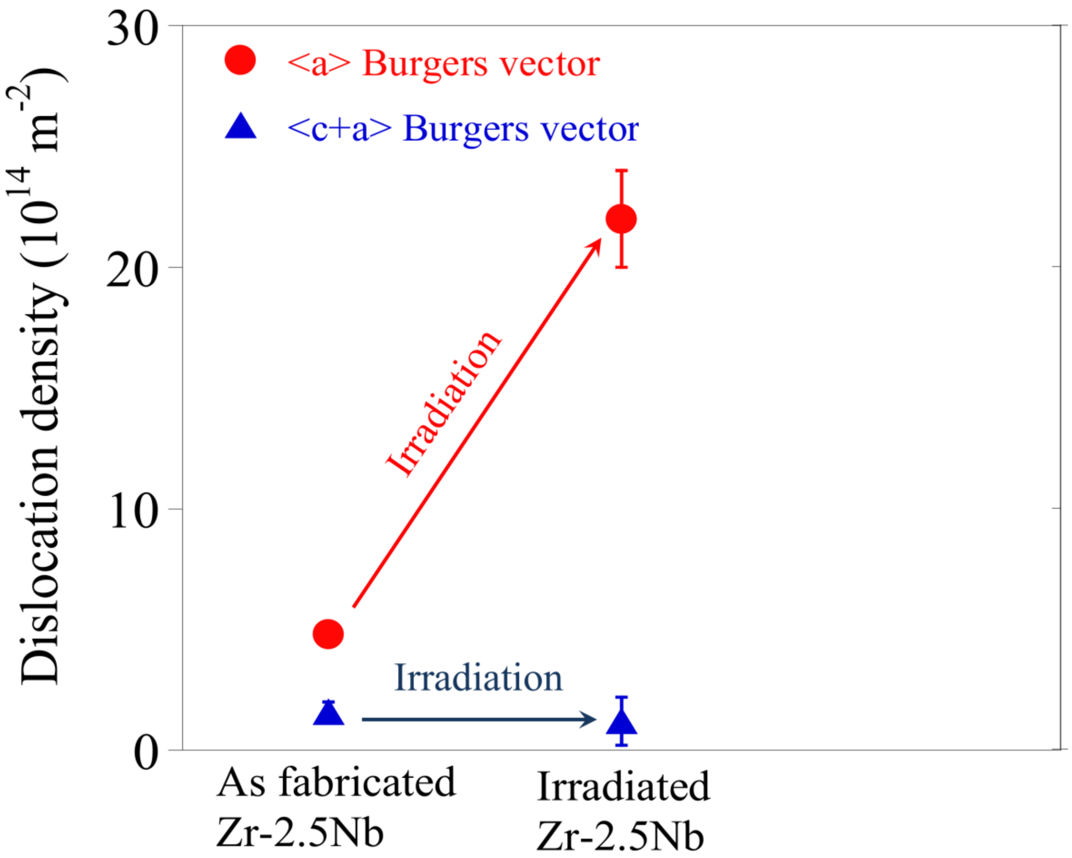

L. Balogh, D.W. Brown, P. Mosbrucker, F. Long, M. R. Daymond, *Acta Mater.*, **60**, (2012) 5567-5577

Example 2: Irradiated HT-9 Steel

FFTF, Hanford site, WA

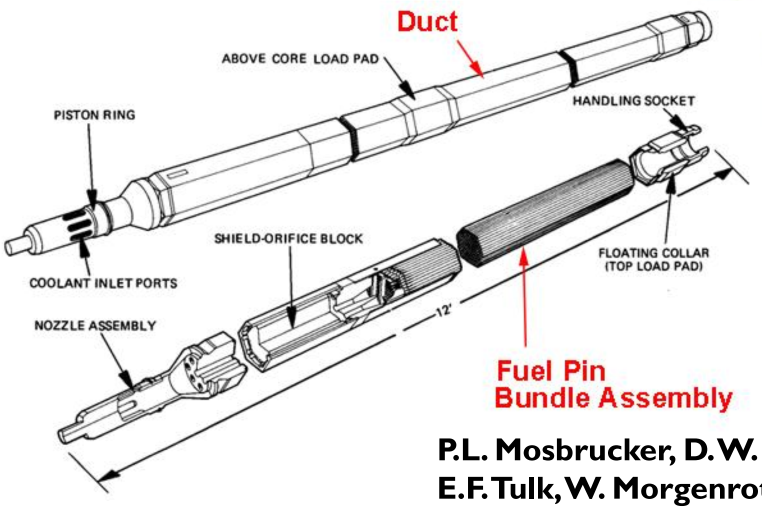

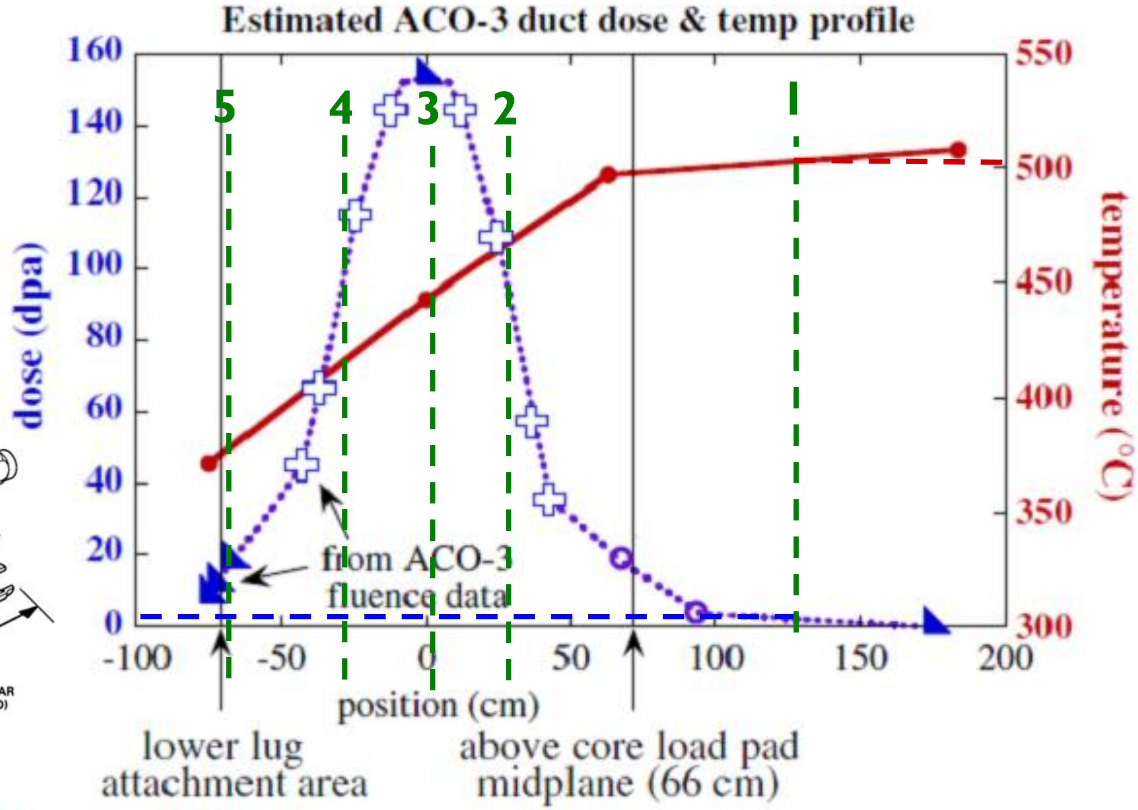

P.L. Mosbrucker, D.W. Brown, O. Anderoglu, L. Balogh, S.A. Maloy, T.A. Sisneros, J. Almer, E.F. Tulk, W. Morgenroth, A.C. Dippel *J. Nucl. Mater.*, **443**, (2013) 522-530.

0.2% yield stress values for irradiated steel samples as a function of irradiation temperature

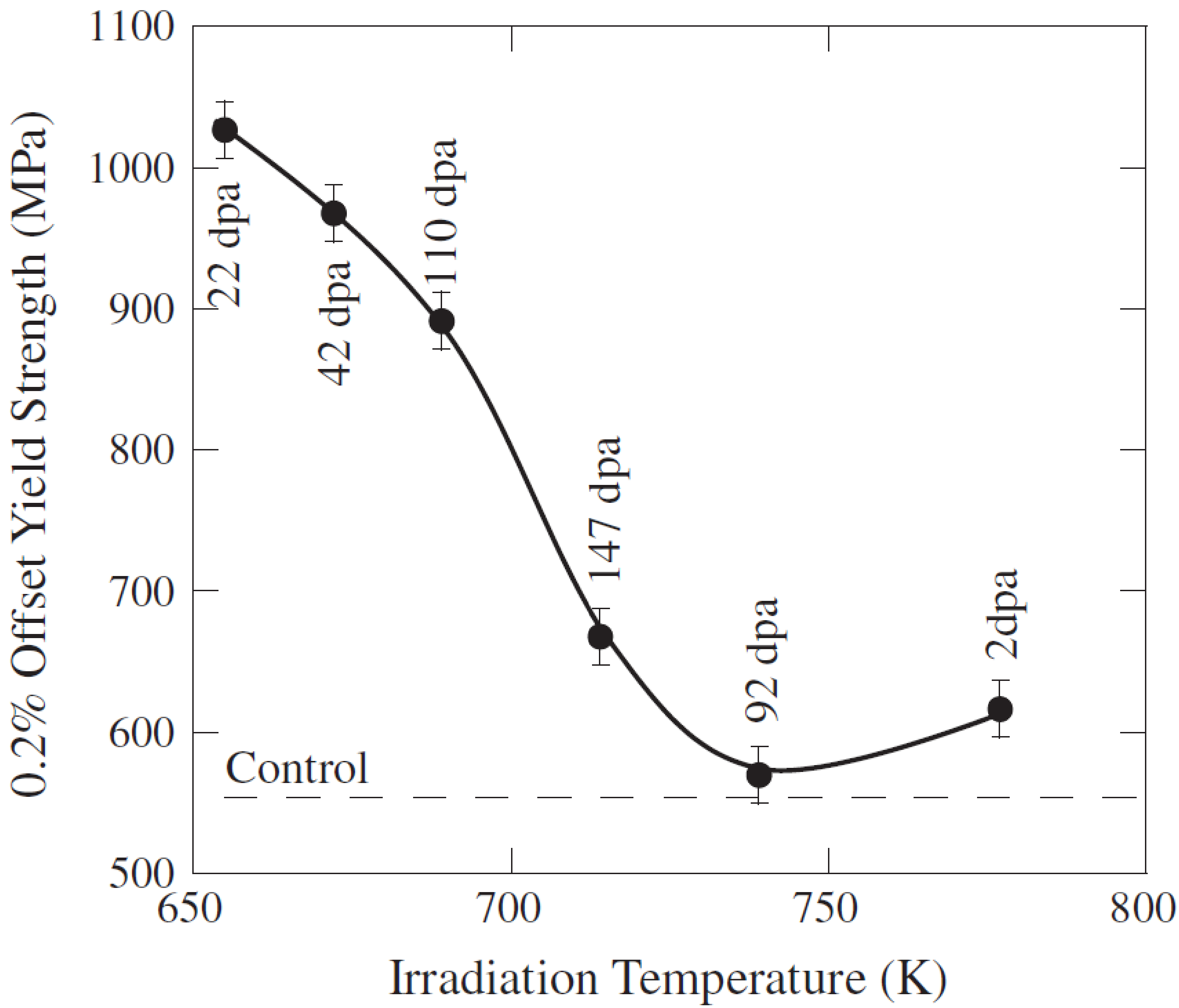

P.L. Mosbrucker, D.W. Brown, O. Anderoglu, L. Balogh, S.A. Maloy, T.A. Sisneros, J. Almer, E.F. Tulk, W. Morgenroth, A.C. Dippel *J. Nucl. Mater.*, **443**, (2013) 522-530.

Significant peak broadening is observed due to the defects created by the irradiation

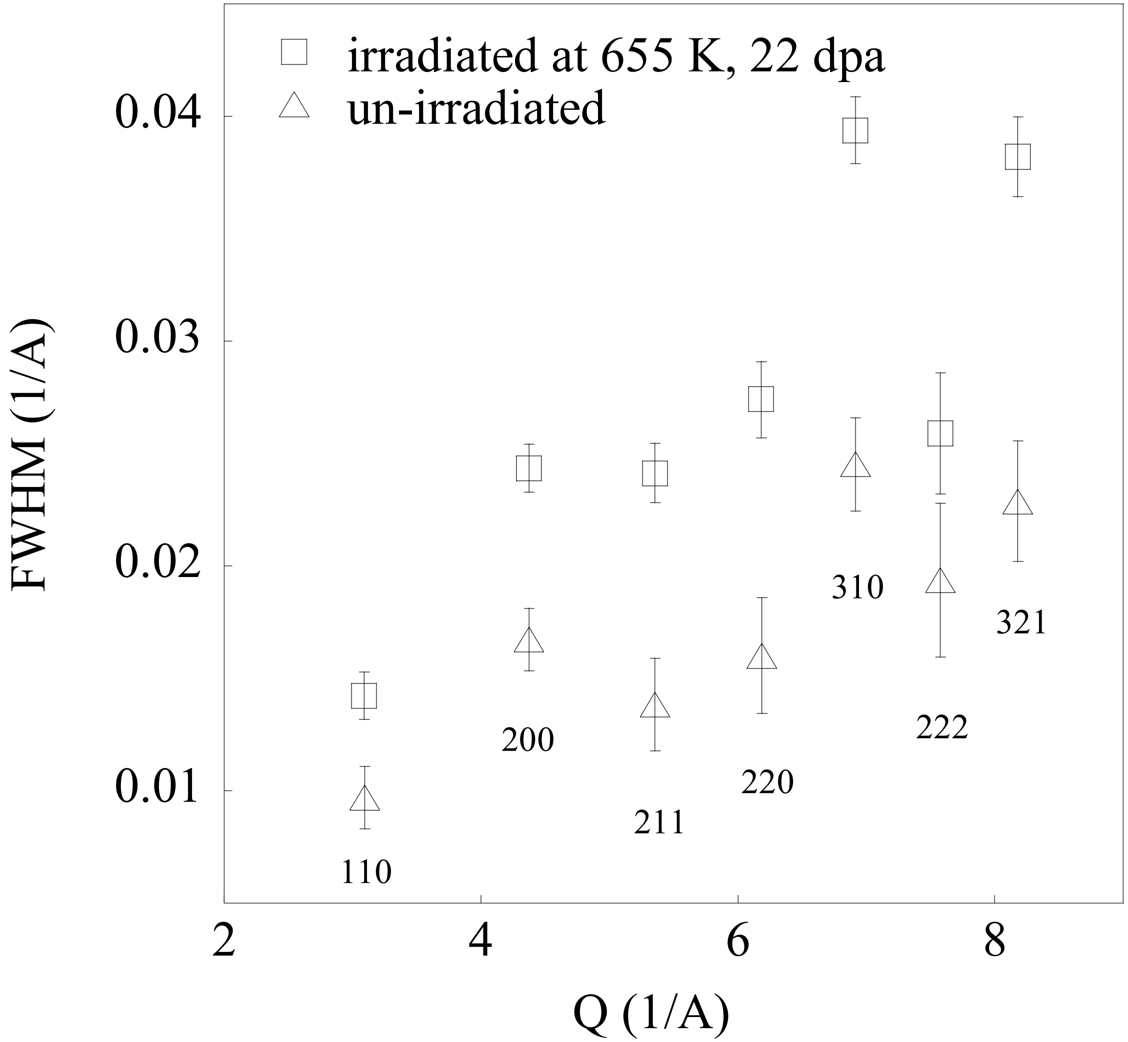

P.L. Mosbrucker, D.W. Brown, O. Anderoglu, L. Balogh, S.A. Maloy, T.A. Sisneros, J. Almer, E.F. Tulk, W. Morgenroth, A.C. Dippel *J. Nucl. Mater.*, **443**, (2013) 522-530.

The microstructure of the irradiated samples are predominantly controlled by the irradiation temperature

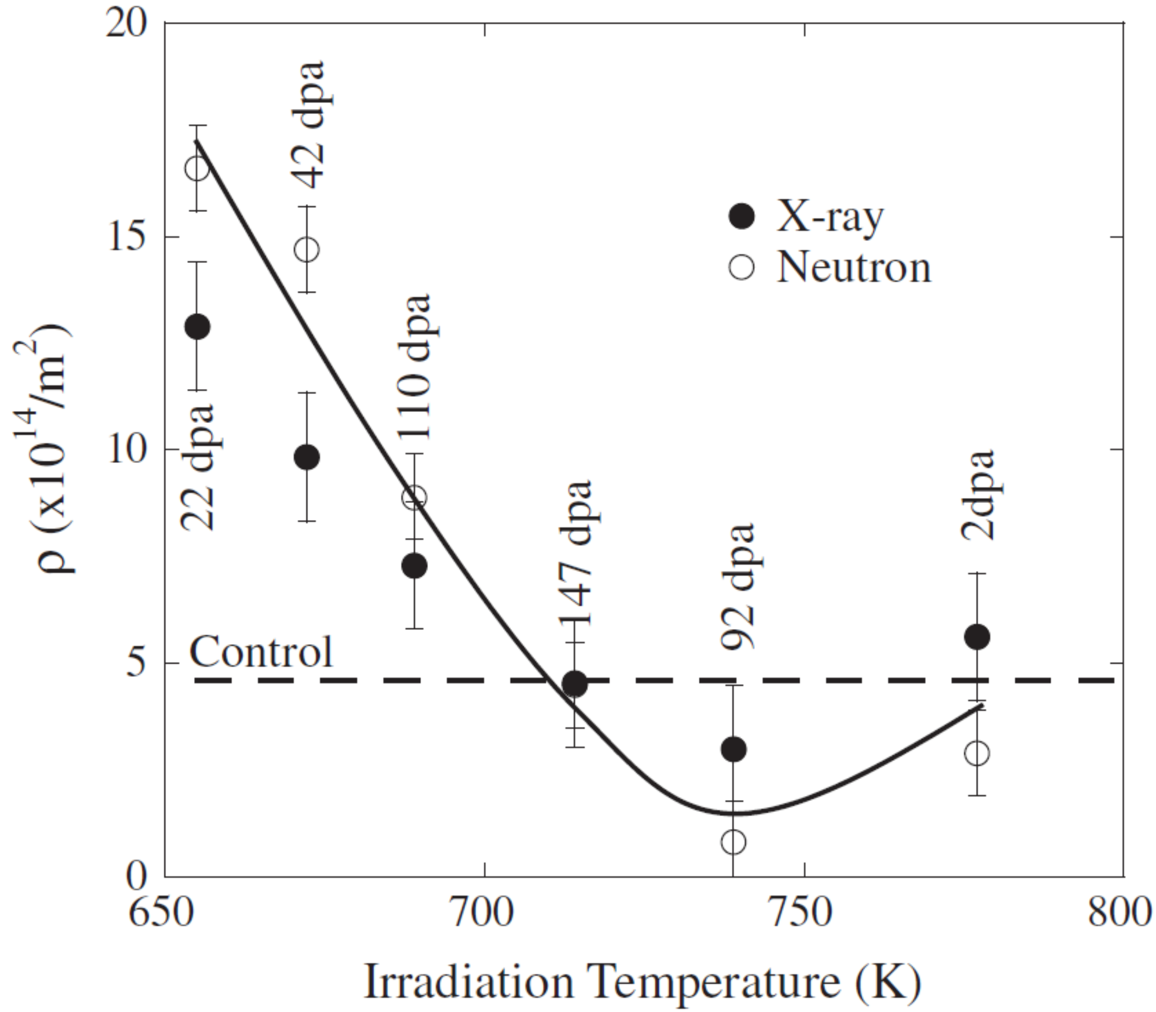

P.L. Mosbrucker, D.W. Brown, O. Anderoglu, L. Balogh, S.A. Maloy, T.A. Sisneros, J. Almer, E.F. Tulk, W. Morgenroth, A.C. Dippel *J. Nucl. Mater.*, **443**, (2013) 522-530.

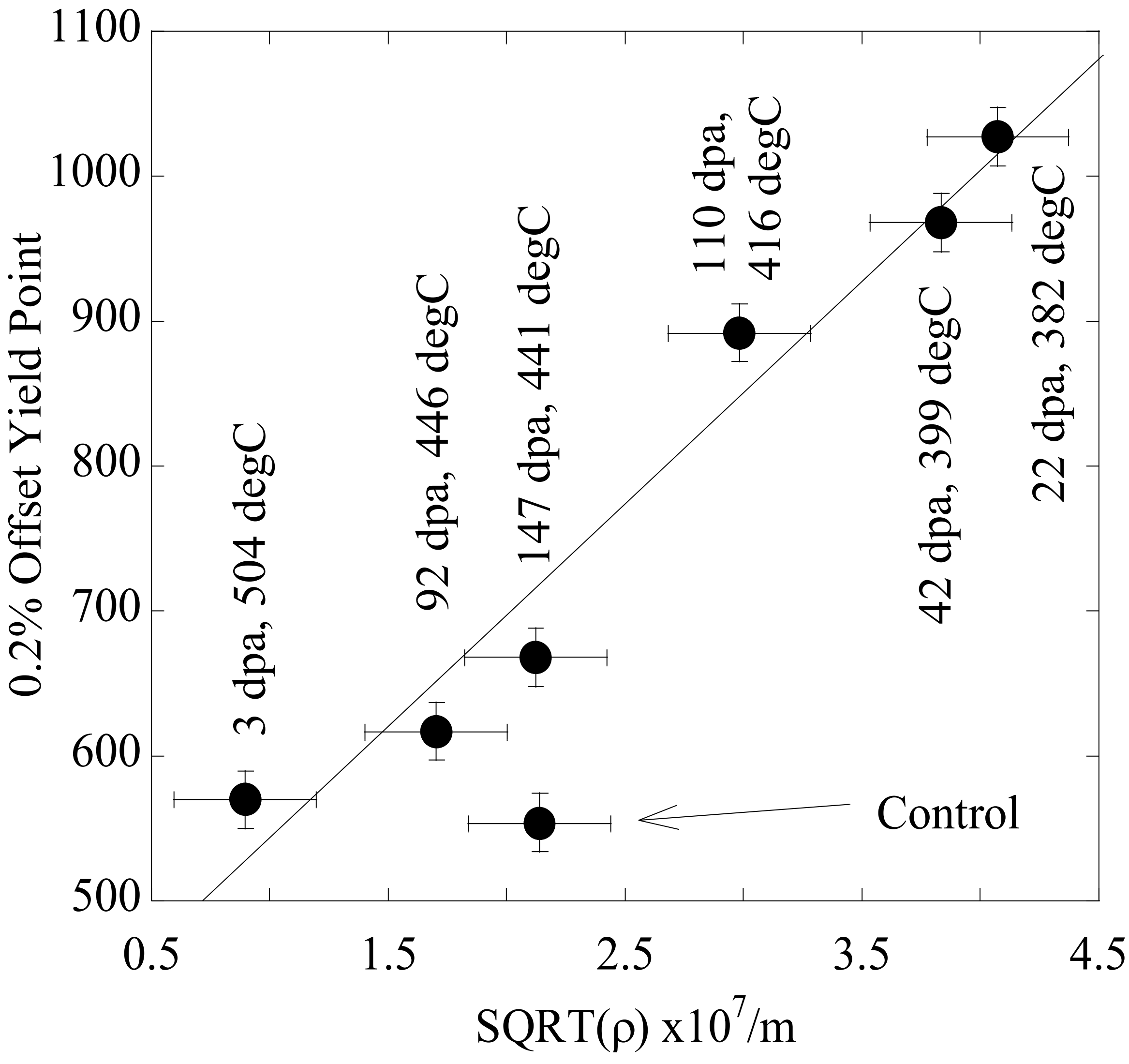

- the dislocation density follows the Taylor equation: estimates of irradiation induced hardening may be obtained from diffraction measurements rather than destructive mechanical tests.

P.L. Mosbrucker, D.W. Brown, O. Anderoglu, L. Balogh, S.A. Maloy, T.A. Sisneros, J. Almer, E.F. Tulk, W. Morgenroth, A.C. Dippel *J. Nucl. Mater.*, **443**, (2013) 522-530.

Conclusions & summary

- Diffraction Line Profile Analysis (DLPA) is a powerful tool for the quantitative characterization of the microstructure.

- Diffraction measurements for DLPA can be non-destructive and can be performed in-situ.

- DLPA and microscopy methods (TEM, SEM, …) are complementary characterization techniques.

Thank you for your attention!

Acknowledgements

Donald W. Brown, LANL
Bjørn Clausen, LANL
Thomas Sisneros, LANL
Kate Page, LANL
Joan Siewenie, LANL
Mark Daymond, Queen's U.
Malcolm Griffiths, AECL
Colin Judge, AECL

AECL
UNENE
COG
Bruce Power
DOE-BES
LANL-LDRD